A Gas Flow-Through System for Hydrogen Isotopic Separation with Metal-Organic Frameworks

Katharine Harp Rigdon

An Honors Thesis presented to
the Department of Physics and Astronomy
of Oberlin College
Adviser: Stephen FitzGerald

April 2019

Executive Summary

In this thesis, we designed and built a gas flow-through system to study dynamic adsorption separation of hydrogen isotopes in metal-organic frameworks (MOFs). MOFs are porous, crystalline materials composed of metal complexes connected by organic linkers. They have been proposed as a cheaper, more energy efficient approach to hydrogen isotope separation than current industrial methods. We have previously found evidence of a zero-point energy-based separation mechanism for hydrogen isotopes in two MOFs: Co-MOF-74 and Cu(I)-MFU-4*l*. This mechanism, chemical affinity quantum sieving (CAQS), has been extensively studied under static equilibrium conditions. The system in this work was developed so that CAQS could be studied under dynamic conditions that more closely resemble those in industrial separation. Breakthrough analysis is an established technique for studying dynamic separation in porous materials. Generally, a breakthrough experiment involves flowing a gas mixture through a fixed bed of adsorbent material and measuring the composition of the effluent flow. In this work, a 1:1 mixture of common hydrogen (H_2) and its isotope deuterium (D_2) was flowed through 71 mg of Co-MOF-74 or 22 mg of Cu(I)-MFU-4*l*. A quadrupole mass spectrometer was used to monitor the composition of the effluent flow. We saw preferential adsorption of D_2 over H_2 in Co-MOF-74 at 77K and Cu(I)-MFU-4*l* at 170K, 140K, and 110K. This behavior was absent in Cu(I)-MFU-4*l* at 77K, a phenomenon that we would like to investigate further. Minimal adsorption occurred in both MOFs at room temperature, as expected. A selectivity of D_2 over H_2 was calculated for each temperature. These selectivities were approximately 30% lower than comparable literature values. Our goal is to make improvements to our system and methods to measure the selectivity more accurately and reproducibly. Notably, all measured selectivities were higher than the selectivity of the Girdler Sulfide method and cryogenic distillation, two industrial hydrogen isotope separation processes we are trying to improve on. This new system gives us the capability to study dynamic

adsorption and kinetic separation of hydrogen isotopes in metal-organic frameworks going forward. We hope that our work will inform the development of efficient, environmentally sustainable separation processes.

To my parents, Caroline and Mark, for being the best support system I could ask for. Thank you for your love and guidance.

Acknowledgements

I am grateful for the people who have contributed to this project and supported me throughout it. First, I want to thank my advisor, Stephen FitzGerald, for being a wonderful professor and mentor over the past two and a half years. His enthusiasm for physics is contagious and working in his lab has been one of the most valuable parts of my Oberlin experience.

I could not have completed this project without the generous assistance of many other Oberlin faculty and staff. The following people deserve many thanks. Matt Elrod lent us a flow meter, supplied us with hydrogen/deuterium gas cylinders (and refilled them when I accidentally vacuumed them out), and nudged me towards the Oberlin Physics Department my freshman year. Mike Miller brought our lab's designs to life in the blink of an eye and entertained many questions about how machines work. Bill Mohler built tricked-out keyboards to automate mundane tasks and always knew how to solve our technical problems. Diane Doman made sure that our lab had the equipment we needed and was an invaluable emotional support system for me throughout my Oberlin education. I also want to recognize all of my Oberlin professors, for challenging me and helping me grow as a student and person.

Additionally, I am grateful for the company of my fellow honors students on this journey. In particular, I want to thank Daniel Mukasa, for designing the temperature controller for these experiments and for his friendship and collaboration over the last four years.

I would also like to thank Dr. Orhan Talu at Cleveland State University and Rebecca Siegelman at University of California-Berkeley for generously showing me their labs, introducing me to the world of breakthrough experiments, and entertaining many questions via email. Jeff Long's group at the University of California-Berkeley synthesized the MOF samples for these experiments and for that I am grateful. This project was funded by NSF Grant #CHE-1565961.

Finally, I would like to thank my family and friends for their constant support and love, even when they got sick of hearing about hydrogen isotopes. I feel incredibly lucky to have them all in my life. Special thanks to Alex Fox, Sarah Brainard, and Hannah Rigdon for editing this thesis.

Contents

List of Figures

List of Tables

Chapter 1

Introduction and Motivation

Increasing energy efficiency in an attempt to reduce carbon emissions and combat climate change is a current focus for many governments and companies globally. The United States consumes 98 quadrillion Btu of energy annually (the equivalent of 17 billion barrels of crude oil)[1]. Industrial gas separations account for 10-15% of this yearly energy consumption[2]. Therefore, there is interest in the development of new industrial gas separation methods that are more energy efficient as well as cost effective than those currently in use.

The separation of gaseous isotopes is uniquely challenging due to their similar size, shape and thermodynamic properties. In this work, we are concerned with the separation of rare hydrogen isotopes deuterium (D_2) and tritium (T_2) from the common protium (H_2) form. All three isotopes contain one proton and one electron but deuterium also contains a neutron while tritium contains two. Deuterium is used as a chemical tracer, in deuterated solvents for NMR spectroscopy, to synthesize more slowly metabolizing drugs, and as a moderator in nuclear reactors (in its heavy water form). Tritium is a radioactive isotope and its removal from nuclear waste is of concern. Tritium also decays into the nucleus ^{3}He, which can be used as a cryogenic

coolant for low-temperature physics[3]. Deuterium and tritium account for 0.0156% and 10^{-17}% of naturally occurring hydrogen, respectively[4, 5].

The industrial separation methods used currently to separate protium and deuterium compounds are the Girdler sulfide process (GS) and cryogenic distillation. The following information on these processes comes from Ref. [6]. GS takes advantage of a difference in chemical reaction rate of hydrogen and deuterium to isolate heavy water, D_2O, from H_2O (containing some D_2O) and H_2S. This process involves hundreds of different separation steps contained in 60m tall towers. The selectivity of this process is 1.3 and it requires 30GJ of energy to produce 1 kg of heavy water. GS is generally used to bring the D_2O content to 20% and then the product is enriched to 99 mol % with cryogenic distillation. This is also an energy intensive process since hydrogen isotopes boil around $\sim$20K; it requires 22 GJ/kg of separated D_2O produced. Cryogenic distillation also has a low selectivity of 1.5. The disadvantages of GS and distillation are that they are both energy intensive and have low selectivity. Additionally, they are used to produce heavy water, not deuterium gas.

We are focused on hydrogen gas separation using membranes and porous materials because of the potential energy efficiency of these processes. In 2016, David Sholl wrote an article entitled "Seven Chemical Separations to Change the World", in which he suggested that membrane-based separation would only use 10% of the energy required for conventional methods such as distillation[2]. Polymers, graphene oxides, carbon molecular sieves, metal-organic frameworks and inorganic membranes such as zeolites are among the different materials under investigation for gas separation applications[7, 8]. In this work, we focus on metal-organic frameworks (MOFs). MOFs are crystalline structures composed of metal complexes connected by organic linkers. Their porous nature and tunability make them a strong candidate for gas separation as they typically have a large internal surface area and their components can be customized for desirable properties. They have been established as a viable

class of materials for separation of acetylene/ethylene, propylene/propane, carbon dioxide/air, and hydrogen isotopes[9, 10, 11, 12]. In addition, many MOFs have been extensively studied for hydrogen storage applications and thus have well-characterized hydrogen adsorption sites[13].

The FitzGerald lab has studied the separation of H_2 and D_2 in MOFs for the past few years[14, 15, 16, 17]. Our current equipment configuration is designed to explore separation through adsorption and desorption processes. The aim of this work is to design a gas flow-through system to look at separation processes based on diffusion and kinetics in addition to adsorption and desorption. Industrial separation processes are generally based on some flow-through method and thus we hope studying MOFs with this new system will inform the development of new industrial separation processes.

1.1 Metal-Organic Frameworks Under Study

As outlined above, metal-organic frameworks are a class of porous materials with high internal surface area which makes them a promising candidate for gas storage and separation applications. They are crystaline structures formed from metal centers connected by organic linkers. The metal centers often contain coordinatively unsaturated metal cations that create adsorption sites for small molecules, like hydrogen. The two MOFs in this work, known as Co-MOF-74 and Cu(I)-MFU-4*l*, were chosen because of their high mass density of adsorption sites and large adsorption energy, respectively[18, 19]. Relevant properties of these MOFs are outlined below.

1.1.1 Co-MOF-74

Co-MOF-74 is part of a group of well-characterized MOFs called M-MOF-74, also known as M_2(dobdc), CPO-27-M, or $M_2(dhtp)_2$[20]. The M-MOF-74 structure was

first synthesized by Rosi et. al. in 2005 with zinc metal centers[18]. Since then, it has also been synthesized with metal centers of magnesium, manganese, iron, nickel and cobalt. The M-MOF-74 structure is capable of adsorbing a large capacity of small molecules due to its high mass density of exposed metal cations[20]. This work looks at Co-MOF-74. It has the chemical formula $C_8H_2Co_2O_6$ and a molar mass of 311.96 g/mol[20]. The structure of a single pore of Co-MOF-74 with adsorbed hydrogen, generated from neutron diffraction data, is depicted in Figure 1.1. The pore diameter is 9.9 Å[21]. The yellow spheres represent adsorbed hydrogen molecules that occupy

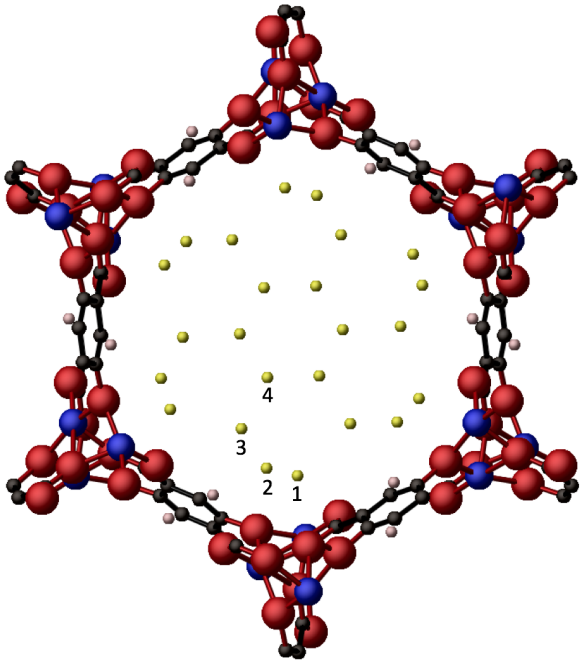

Figure 1.1: Structure of one pore of Co-MOF-74. Blue spheres represent cobalt atoms, black represent carbon, red represent oxygen, and pink represent hydrogen. The yellow spheres represent adsorbed hydrogen molecules, which occupy four adsorption sites associated with each cobalt. The sites are labeled in order of decreasing adsorption strength. The figure was generated from neutron diffraction data in Ref. [20].

four distinct sites per cobalt cation. The sites are labeled in order of decreasing adsorption strength.

In their 2011 paper, FitzGerald et al. showed that the hydrogen adsorption sites of M-MOF-74 fill sequentially when loading at low pressure and temperature [22]. The primary sites fill first, followed by the secondary, etc. The primary site, also referred to as the open metal site, has the highest isosteric heat of adsorption at 10.8kJ/mol[20]. This leads to the adsorption of hydrogen and deuterium around 100K at low pressure [16].

1.1.2 Cu(I)-MFU-4*l*

Cu(I)-MFU-4*l* is a member of the MFU-4*l* framework family in which some Zn(II)–Cl units have been replaced with Cu(I) ions (Fig. 1.2). The MFU-4*l* structure is a larger-pore derivative of the MFU-4 structure and was first synthesized in 2011 [23]. The chemical formula of Cu(I)-MFU-4*l* is $C_{36}H_{12}Cl_4N_{18}O_6Cu_2Zn_3$ and its molar mass is 1257.7 g/mol [19].

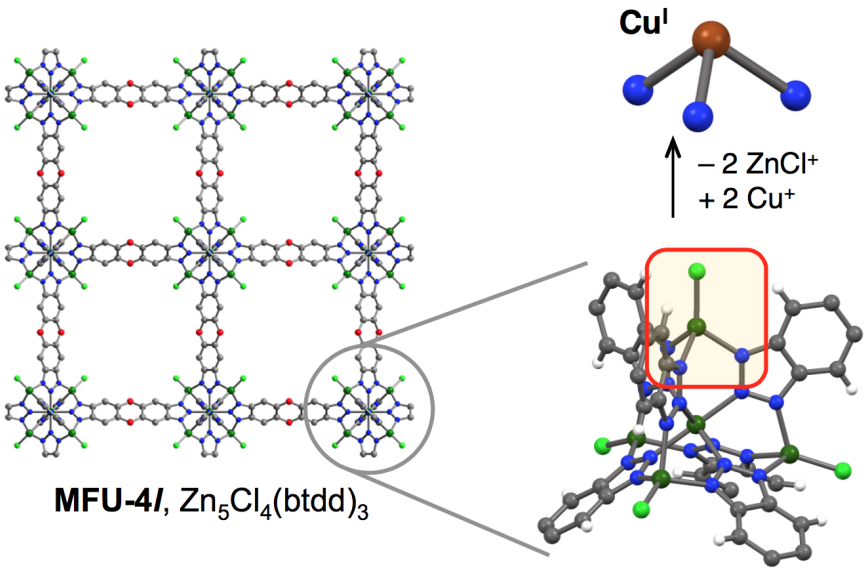

Figure 1.2: Cu(I)-MFU-4*l* synthesis from MFU-4*l*. Two of the four tetrahedral sites are replaced with Cu(I). Figure from Ref. [24] with data from Refs. [19, 23].

Figure 1.3, depicting the structure of Cu(I)-MFU-4*l*, is taken from Ref. [3]. Fig. 1.3a shows a single pore of Cu(I)-MFU-4*l*. Ref. [23] found the pore aperture to be 9.1 Å, which is much larger than the original MFU-4 structure. Figure 1.3b depicts a model of hydrogen adsorption in Cu(I)-MFU-4*l*. This MOF is of particular interest because it has an isosteric heat of adsorption of 32.7 kJ/mol, which is close to the proposed 25 kJ/mol target for practical room-temperature hydrogen adsorption (and desorption)[3, 19]. In practice, we have found that hydrogen desorbs around 220K [14]. Though it has a high isosteric heat of adsorption, Cu(I)-MFU-4*l* only has a quarter of the number of adsorption sites per gram as Co-MOF-74.

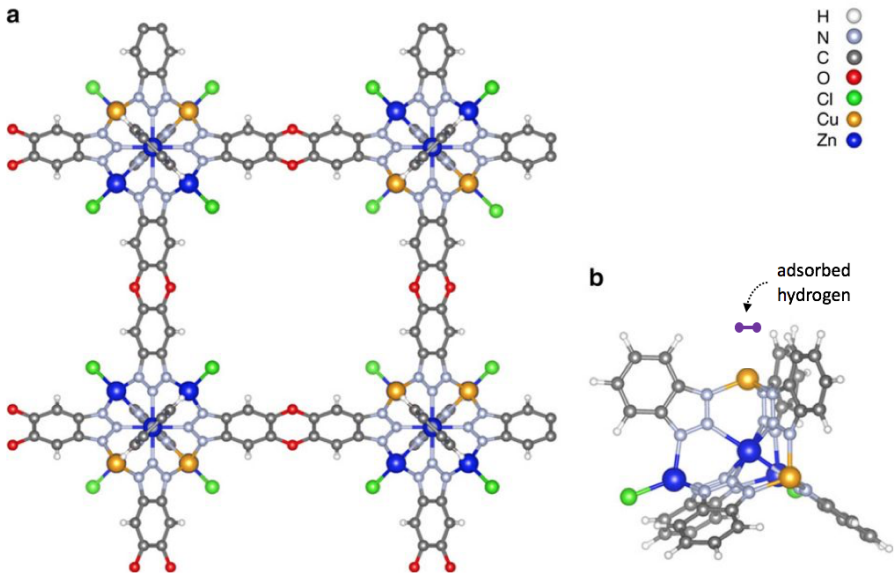

Figure 1.3: Figure adapted from Ref. [3]: **a.** Structure of a single pore of Cu(I)-MFU-4*l*. Atomic color scheme is depicted in the upper right. **b.** Model of adsorbed hydrogen in the Cu(I) open-metal site.

Chapter 2

Background

2.1 Separation Mechanisms in Porous Materials

Utilizing porous materials such as MOFs has been proposed as a cheaper, more energy efficient approach to hydrogen isotope separation[25]. Two separation mechanisms that depend on the quantum properties of MOF-hydrogen interactions have been proposed in the literature. Chemical affinity quantum sieving (CAQS) and kinetic quantum sieving (KQS), are outlined below[12]. From this point forward, this work will specifically discuss the separation of H_2 and D_2 isotopes, as they are the simplest to work with in a laboratory. In principle, these mass-based mechanisms could also be applied to T_2-H_2 separation.

2.1.1 Chemical Affinity Quantum Sieving (CAQS)

Chemical affinity quantum sieving (CAQS) is the main separation method investigated in this work. This method takes advantage of the difference in the chemical affinity of hydrogen isotopes for the adsorption sites in a MOF. In general, this difference leads to the preferential adsorption of more massive isotopes over less massive ones[12]. Zero point energy separation (ZPES) is perhaps a more fitting name for this

method, since it is mainly a difference in translational zero point energy that leads to the preferential adsorption of more massive isotopes[17]. Assumming the translational energy of adsorbed hydrogen can be approximated as a 3-D simple harmonic oscillator, its zero-point energy (ZPE) is defined according to:

$$E_0 = \frac{3}{2}\hbar\omega. \tag{2.1}$$

Here, $\hbar$ is the reduced Planck constant and ω is the angular frequency of the molecule. The angular frequency is related to the mass of the molecule according to the equation

$$\omega = \sqrt{\frac{k}{m}} \tag{2.2}$$

where k is a spring constant and m is the mass of the gas molecule. We can assume that for any adsorption site k, the second derivative of the potential energy in the binding site, is the same for all hydrogen isotopes since they are practically chemically identical. However, the isotopes differ in mass due to the number of neutrons they contain and therefore they have different ZPEs. The heavier the isotope, the smaller its ZPE and the larger the resultant binding energy[17]. The difference in binding energy between isotopes is the difference in their zero point energy. In the case of H_2 and D_2, with the approximation that $\omega_{D_2} = \frac{\omega_{H_2}}{\sqrt{2}}$,

$$\Delta ZPE = \frac{3}{2}\hbar\omega_{H_2}(1 - \frac{1}{\sqrt{2}})[17]. \tag{2.3}$$

Experimentally, ΔZPE is measured from a difference in the isosteric heat of adsorption (Q_{st}). Q_{st} is a temperature-dependent measure of the heat lost by a molecule as it transitions from the gas phase to the adsorbed phase. It can be measured from adsorption at different temperatures. In the limit as the temperature approaches absolute zero, Q_{st} is equivalent to the binding energy[17]. Figure 2.1 depicts Q_{st},

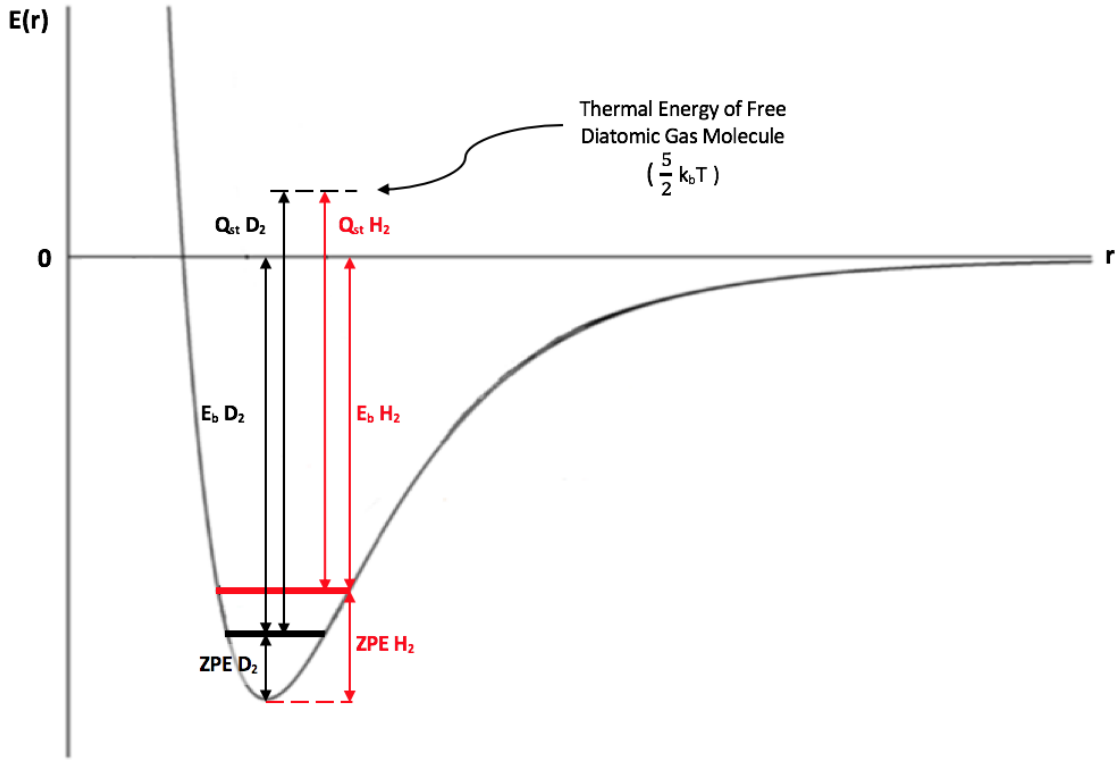

Figure 2.1: Depiction of Q_{st}, binding energy (E_b), and ZPE for adsorbed H_2 and D_2 at an arbitrary temperature in a generic 1-dimensional potential (where r is the physical location of the adsorbed molecule). Adapted from Ref. [17].

binding energy (E_b), and ZPE for adsorbed H_2 and D_2 at an arbitrary temperature in a generic 1-dimensional potential (where r is the physical location of the adsorbed molecule).

Based on the known translational energy of hydrogen, we can assume that almost all adsorbed hydrogen isotopes are in their ground translational state below 200K. The selectivity of the CAQS separation mechanism, assuming adsorbed hydrogen is a SHO, can be approximated as

$$S = e^{\Delta ZPE/k_B T} \tag{2.4}$$

where k_B is the boltzmann constant and T is temperature. Eq. 2.4 indicates that the selectivity increases as temperature decreases. Experiments have shown that this is true for both Co-MOF-74[17] and Cu(I)-MFU-4l[3].

The separation of hydrogen isotopes due to CAQS in MOFs has been extensively studied in the FitzGerald lab. Previous honors studies using infrared and thermal-desorption spectroscopy can be found in Refs. [16] and [14]. A Q_{st} measurement from isotherms for Co-MOF-74 is published in Ref. [17].

2.1.2 Kinetic Quantum Sieving (KQS)

Kinetic quantum sieving (KQS) is a separation mechanism based on a difference in de Broglie wavelength of hydrogen isotopes. It was first proposed by Beenakker et al. in 1995[26]. Porous materials are suitable for KQS if the size of the entrance pores is comparable to the de Broglie wavelength of the molecules intended for separation[25]. In this regime, there is a higher diffusion barrier for lighter isotopes. At sufficiently low temperatures, the difference in molecular diffusivity can be large enough such that significant isotope separation occurs[12]. Oh et al. suggested that the optimal pore size for H_2/D_2 separation via KQS is between 3.0 Å and 3.4 Å[27]. Ref. [12] outlines some experimental studies on KQS for H_2 and D_2 in MOFs. So far, the observed differences in diffusivity at 77K between H_2 and D_2 have been small in traditional MOFs, with selectivities below 1.5[28]. High selectivity has only been observed at minimal coverage pressure and low temperature (20K)[27]. Temperature-triggered flexible MOFs have shown the best results, with selectivities up to 7.5 at 60K and 10mbar[29].

Co-MOF-74 and Cu(I)-MFU-4l, the MOFs in this work, have pore sizes around 9 Å that are too large for KQS of hydrogen isotopes. However, the flow-through system developed in this work could be used to study KQS with smaller pore MOFs in the future.

2.2 Breakthrough Analysis

Previous study of adsorption separation in MOFs in the FitzGerald lab has been conducted under static equilibrium conditions. Interest in characterizing adsorption separation under dynamic conditions that more closely resemble those in industrial separation led us to breakthrough analysis. Breakthrough analysis, also known as frontal chromatography, is a well-established technique that has been used to study gas separations in MOFs[30, 31, 32] and hydrogen isotopic separation in zeolites[33]. To the author's knowledge, this technique has not been used to study hydrogen isotope separation in MOFs.

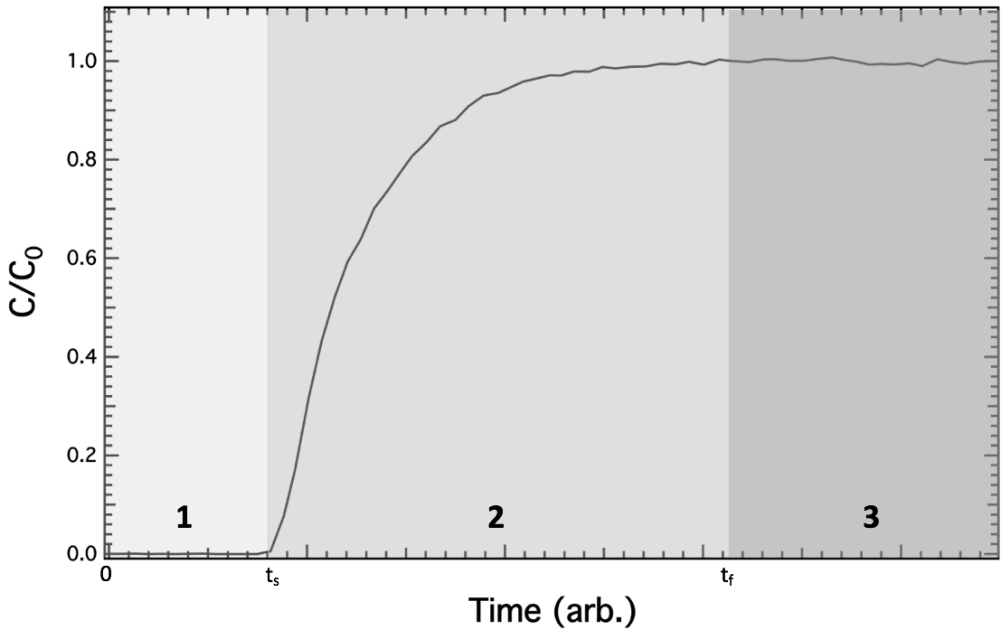

Figure 2.2: Phases of a single component breakthrough curve: 1- gas is fed into the adsorbent bed at a known rate with concentration C_0 and is entirely adsorbed; t_s- time at which C/C_0 begins to rise, referred to as the initial breakthrough time; 2- gas begins to make it through the adsorbent without being adsorbed and the concentration ratio in the effluent flow rises; t_f- time at which C/C_0 reaches 1, referred to as the complete breakthrough time; 3- C/C_0 is 1 and the system is at equilibrium.

In general, a breakthrough experiment involves flowing a gas mixture (the feed) across a fixed bed of porous adsorbent and measuring the composition of the efflu-

ent flow with a mass spectrometer or gas chromatograph. The specific experimental procedure used in this work is outlined in Chapter 3. The adsorption capacity, selectivity, and kinetics of the adsorbent can be measured through breakthrough analysis as long as the flow rate of the feed and composition of both the feed and effluent flow are known. Figure 2.2 shows a typical single component breakthrough curve (the feed contains a single adsorbate). The ratio of the concentration of the adsorbate in the effluent flow (C) to the feed concentration (C_0) is plotted against time. In phase 1, gas is introduced to the adsorbent at a known, constant flow rate and is entirely adsorbed, so C/C_0 is 0. Phase 2 begins at the initial breakthrough time (t_s), the time at which gas begins to make it all the way through the bed of adsorbent. Throughout phase 2, C/C_0 rises until it reaches 1 at t_f, the complete breakthrough time[33]. In phase 3, C is equal to C_0 and the system has come to equilibrium.

The number of moles of the adsorbate retained in the adsorbent bed can be calculated from the data in Fig. 2.2 according to the equation

$$n_{ads} = FC_0 \int_0^\infty [1 - \frac{C(t)}{C_0}]dt \tag{2.5}$$

where F is the flow rate [cm^3/min], C_0 is the input concentration [mol/cm^3], and C(t) is the concentration of the effluent flow at any time t [min][34]. This is a measure of the adsorption capacity of the material at the pressure established by the flow rate. It is an approximation of the amount of feed adsorbed because this calculation technically includes gas retained in the dead space of the adsorbent in addition to the gas in adsorption sites.

Phase 2, sometimes called the mass transfer region, contains information about the kinetics of a breakthrough experiment. Generally, understanding of the kinetics of a breakthrough experiment is obtained by comparing theoretical models to the data. Three commonly used kinetic breakthrough models are the Thomas[35], Yoon-

Nelson[36], and Adams-Bohart models[37]. Well-correlated fits to these models can be used to calculate parameters like the maximum adsorption capacity, mass transfer coefficients, and rate constants[38, 39].

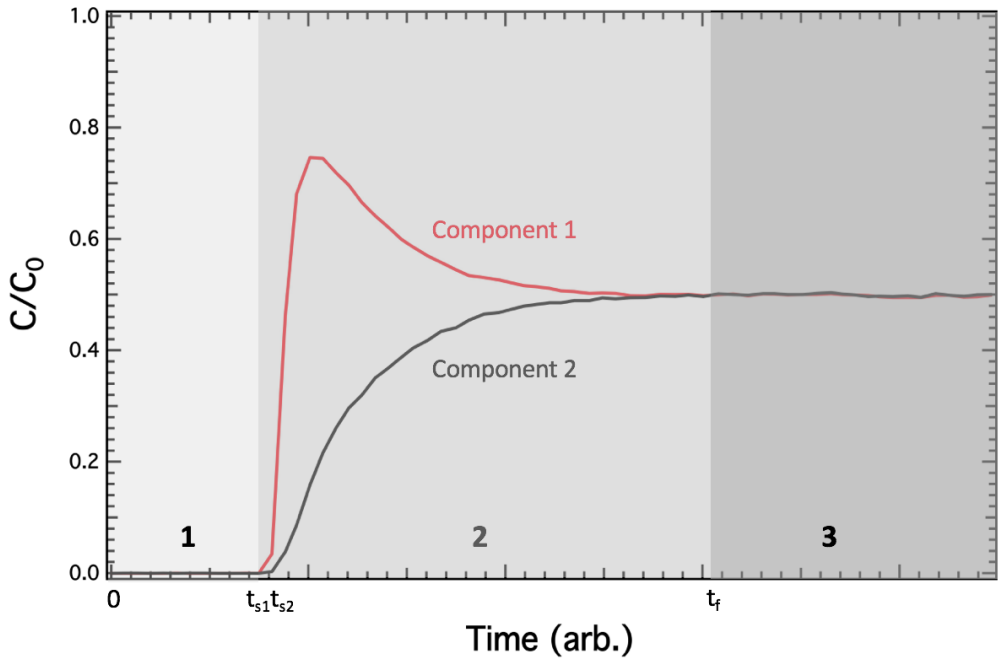

Figure 2.3: Phases of typical two-component breakthrough curve where component 2 is preferentially adsorbed (composition of feed mixture is 1:1): 1- mixture is fed into the adsorbent bed at a known rate and is entirely adsorbed; t_{s1} and t_{s2}- initial breakthrough times of Component 1 and 2, respectively; 2- Component 1 breaks through first, and is displaced by Component 2, which has a later breakthrough time; 3- system comes to equilibrium at $C/C_0 = 0.5$. C_0 is defined as the total input concentration.

Breakthrough experiments with a mixture feed can be used to evaluate the separative capabilities of an adsorbent. Figure 2.3 shows a typical breakthrough curve for a 2-component feed (1:1 composition) where Component 2 is preferentially adsorbed. Here, C_0 is the total input concentration and each component has an individual input concentration of 0.5 C_0. The difference in initial breakthrough time between components (t_{s1} and t_{s2}) and the overshoot of Component 1 (the region where C/C_0 exceeds 0.5) are evidence of preferential adsorption. The overshoot (sometimes called roll-over) effect happens because adsorbed Component 1 is displaced by Component

2, resulting in a C/C_0 higher than 0.5 towards the beginning of the mass transfer region (phase 2)[40]. In general, maximizing the mass transfer region (with respect to time) is desirable for separation applications because the difference in initial breakthrough time between separable mixture components is maximized and subsequently, the adsorbent doesn't need to be regenerated as often[33]. The time scale of the mass transfer region varies with temperature, flow rate, initial concentration, and choice of adsorbent.

A 2-component breakthrough curve can be used to calculate the selectivity of the adsorbent bed. Selectivity is generally defined as

$$S_{2/1} = \frac{n_{2ads}/n_{2gas}}{n_{1ads}/n_{1gas}}, \tag{2.6}$$

the ratio of the moles of adsorbed Component 2 (n_{2ads}) to gas phase Component 2 (n_{2gas}) divided by the same ratio for Component 1. In this work, n_{1gas} and n_{2gas} are equivalent, so our selectivity is a ratio of n_{2ads}/n_{1ads}. For a 2-component breakthrough experiment, n_{ads} is

$$n_{ads} = FC_0 \int_0^\infty [0.5 - \frac{C(t)}{C_0}]dt \tag{2.7}$$

where C_0 is the total input concentration and all other variables are consistent with Eq. 2.5. Combining Eq. 2.7 and Fig. 2.4, the selectivity is

$$S_{2/1} = \frac{\text{Area}(a+b)}{\text{Area}(a-c)}. \tag{2.8}$$

Eq. 2.8 is a simplified version for a 1:1 feed mixture in which the flow rate and initial concentration of the two components is the same. This is the selectivity of the gas retained in both the adsorption sites (the selective volume) as well as the interparticle voids and nonselective pores (the non-selective volume) of the adsorbent.

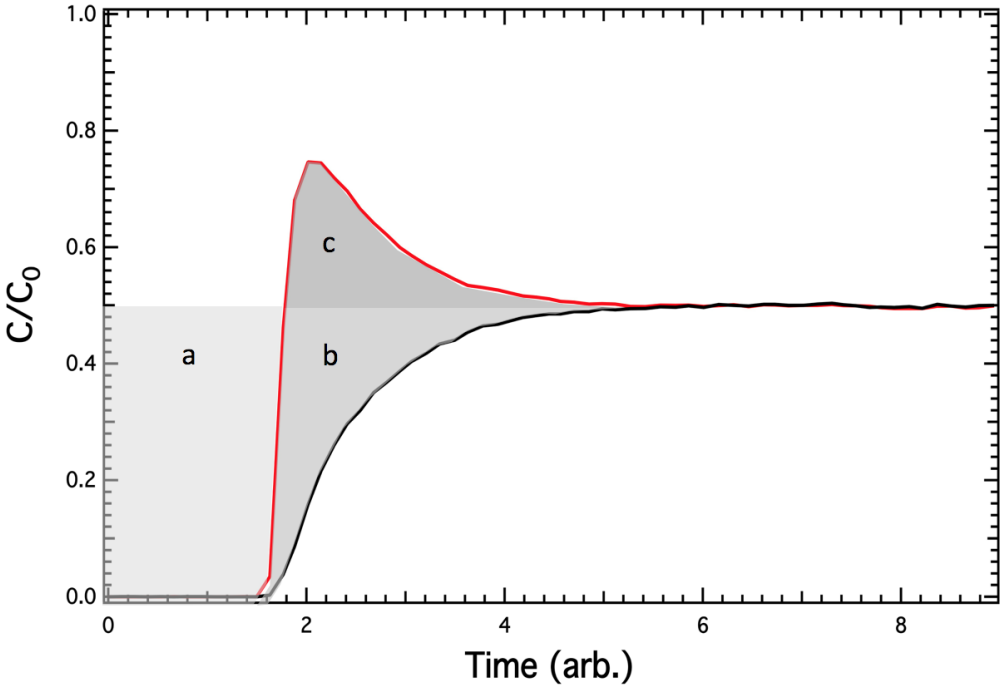

Figure 2.4: Selectivity can be calculated as a molar ratio of adsorbed Component 2 (Area$(a+b)$) to adsorbed Component 1 (Area$(a-c)$). Figure adapted from Ref. [34].

Ref. [34] outlines a method to calculate the selectivity of just the selective volume of the adsorbent. Eq. 2.8 is modified with a term that eliminates the gas trapped in the non-selective volume:

$$S_{2/1} = \frac{\mathrm{F}\times\ \mathrm{Area}(a+b) - V_{ns}C_0}{\mathrm{F}\times\ \mathrm{Area}(a-c) - V_{ns}C_0}. \tag{2.9}$$

Here V_{ns} is the nonselective volume of the adsorbent [cm^3], which can be experimentally determined with a non-adsorptive gas. Eq. 2.9 can be simplified to:

$$S_{2/1} = 1 + \frac{\mathrm{F}\times\ \mathrm{Area}(b+c)}{\mathrm{F}\times\ \mathrm{Area}(a-c) - V_{ns}C_0}. \tag{2.10}$$

Control over the temperature of the adsorbate bed is important in a breakthrough experiment. The CAQS effect is more selective at lower temperature, so most of the experiments in this work are run with the MOF sample between 180K and 77K.

Managing the temperature of the MOFs is a potential challenge because of their large isosteric heats of adsorption at low temperature. When they adsorb gas, heat is released which may significantly raise the temperature of the MOF and diminish CAQS separation effects.

In terms of ease of separation, breakthrough experiments provide a simple mechanism for the recovery of the less preferentially adsorbed components of a mixture. Adjustments must be made to the generic breakthrough experiment to isolate the more preferentially adsorbed species. In this work, the desire is to isolate deuterium, the more strongly adsorbed species. Therefore, developing the capacity to conduct breakthrough experiments (the focus for this thesis) is only the first step in developing a method for isolating deuterium. Processes like Pressure and Temperature Swing Adsorption (PSA and TSA) can be used to strategically recover deuterium[41, 42].

2.3 Mass Spectrometry

Mass spectrometry is the technique used to monitor the composition of the effluent flow during breakthrough experiments in this work. This section reviews the basic principles behind mass spectrometry while Ch. 3 provides details on the specific quadrupole mass spectrometer used.

Figure 2.5 depicts the main three components of a quadrupole mass spectrometer: the ionization chamber, mass filter, and detector. The following description was informed by Ref. [44]. A sample of the effluent flow is pulled into the ionization chamber, where beams of electrons convert gas molecules into positively charged ions and electrons. The charged particles are accelerated to the same kinetic energy and directed into the quadrupole mass filter. The filter consists of two sets of parallel rods kept at equal but opposite potentials with a combination of a fixed DC and alternating RF component. As ions enter the mass filter, they are deflected by the

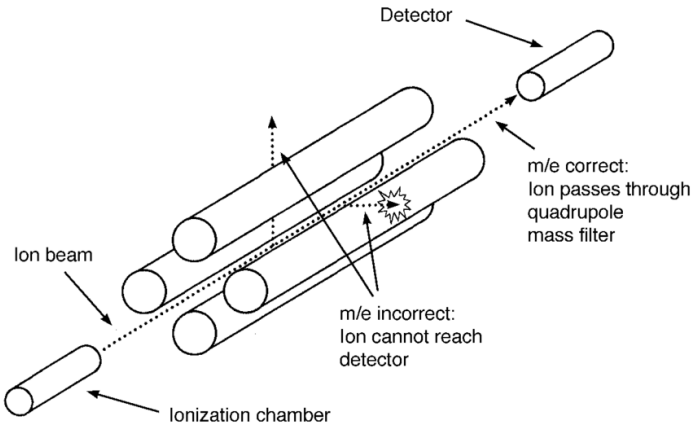

Figure 2.5: Main components of a quadrupole mass spectrometer: ionization chamber, quadrupole, and detector. Select particles reach the detector based on m/e ratio. Figure from Ref. [43].

electric field created by the rods depending on their mass to charge ratio. The RF component of the potential is set so that only particles of a specific mass make it through the filter to the detector at the other end. The other particles are deflected into the rods and neutralized. The setting of the RF component can be altered quickly so that the concentration of multiple gases in a mixture can be analyzed in real time. The two detectors used in the mass spectrometer in this work are a faraday cup and a secondary electron multiplier. Both operate on the same basic principle that when an ion hits the detector, it generates a cascade of electrons that amplifies the signal and allows for a measurement of the concentration of a specific mass[45].

Chapter 3

Experimental Apparatus and Procedure

The following chapter details the equipment, setup, and procedures used to conduct breakthrough experiments.

3.1 Experimental Setup

Fig. 3.1 shows the experimental setup, with the red outline designating equipment that was added to the system over the course of this project. The Micromeretics ASAP (Accelerated Surface Area and Porosimetry) 2020 gas dosing system, the Hiden HPR-20 Quadrupole Mass Spectrometer and the 1/8" copper tubing connecting them were original to the system. During the breakthrough experiments, the ASAP was used to feed the system with pure H_2, D_2, or He and monitor the pressure upstream of the sample. A 1:1 H_2/D_2 mixture, used as the feed for most of our breakthrough experiments, was contained in a 500cm^3 cylinder separate from the ASAP. A Sierra SmartTrak 50 Mass Flow Meter was used to monitor the feed flow rate. The flow rate was controlled with a Swagelok needle valve just downstream of the flow meter.

A Swagelok 3-way ball valve was used to direct the flow through the sample or to bypass it.

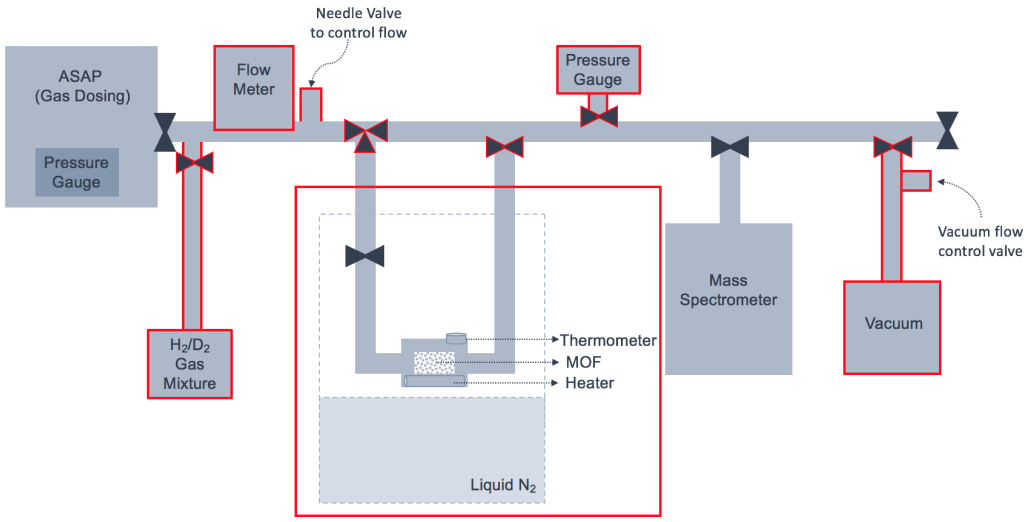

Figure 3.1: Components of the breakthrough experiment system; red outline designates equipment added over the course of this project. Gas flows into the system from the ASAP or H_2/D_2 mixture cylinder at a rate controlled by the needle valve. The flow is measured with a flow meter and directed through or around the MOF sample with a 3-way valve. The temperature of the sample is controlled with a combination of a heater and liquid nitrogen vapor. The pressure and composition of the effluent flow are measured with a pressure gauge and a mass spectrometer. The excess flow leaves the system through a vacuum.

Two MOF sample cells, pictured in Fig. 3.2, were designed for this experiment. Fig. 3.2a. shows the first cell, used in the Co-MOF-74 breakthrough experiments. The limitation on this cell design is that breakthrough experiments can only be conducted at temperatures attainable with cooling baths (room temperature and 77K in this work). The second cell, pictured in Fig. 3.2b. and shown in Fig. 3.1, was designed by Daniel Mukasa and can maintain the MOF sample at temperatures between room temperature and 100K. More details on this apparatus can be found in Ref. [46]. This cell was used for the experiments with Cu(I)-MFU-4*l*.

An Omega general purpose pressure gauge was used to measure the pressure downstream of the sample. The mass spectrometer was used to monitor the composition of

the effluent flow. The mass spectrometer was not capable of processing the entirety of the effluent flow in real time and so a Leybold-Heraeus D4A vacuum pump was used to prevent pressure from building downstream of the sample. Just upstream from the vacuum, a Swagelok flow metering valve gave us adjustable control over the vacuum rate. Swagelok bonnet valves were used throughout the system to control the path of the flow.

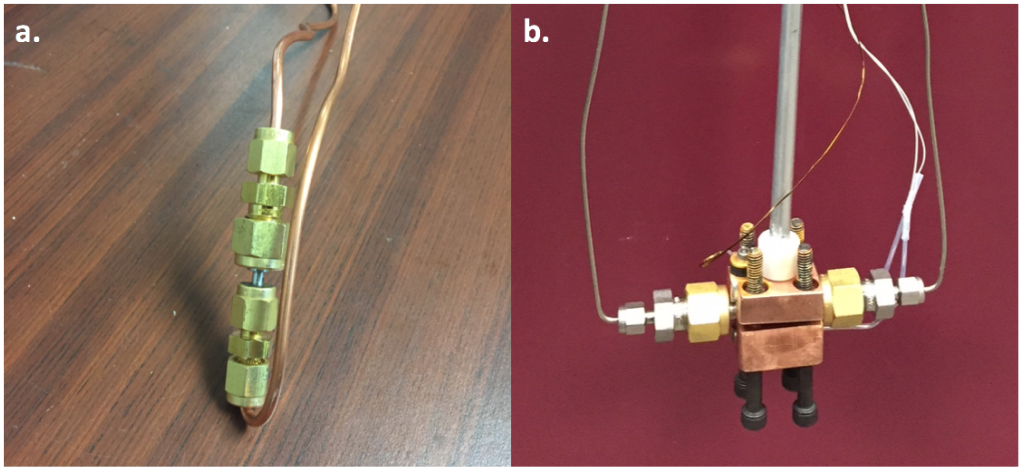

Figure 3.2: **a**. Basic sample cell used in Co-MOF-74 experiments; MOF sample is held in the stainless steel cell between the brass Swagelok connections. **b**. Temperature-controlled sample cell used in Cu(I)-MFU-4*l* experiments; sample is held in an aluminum cell surrounded by a copper cube outfitted with a heating element and a temperature probe.

3.2 Preparation of MOF Column

Both the Co-MOF-74 and Cu(I)-MFU-4*l* powder samples were synthesized by Jeff Long's group at the University of California-Berkeley. All handling of MOF samples was done in an argon-filled glove box. When making a MOF column, the powder sample was weighed and then hand-packed into one of the cells pictured in Fig. 3.2. Fig. 3.3 shows (1) the base that held the cell, (2) the aluminum funnel used to load the powder into the cell, and (3) the plungers used to gently press the powder

into a pellet that filled the cell and stayed in place when the apparatus was moved. Considerations for MOF column synthesis in the future can be found in Appendix A.

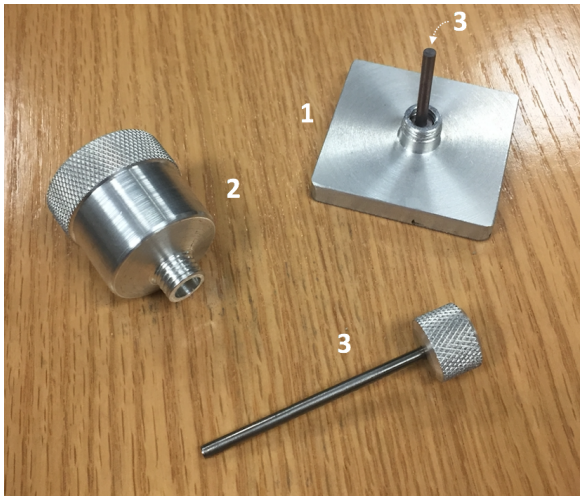

Figure 3.3: Tools used to prepare MOF column: 1- base to hold cell; 2- funnel to load powder into cell; 3- plungers used to gently hand-press the pellet.

3.3 Preparation of 1:1 H_2/D_2 Mixture

A 1:1 H_2/D_2 gas mixture at 2 atm in a 500 cm^3 cylinder was used as the feed for all experiments presented in Ch. 4. Dr. Matt Elrod in the Oberlin Chemistry Department prepared this mixture for us with a vacuum system connected to H_2 and D_2 supply tanks with regulators. The vacuum was used to evacuate the system, including the cylinder. The system was then isolated from the vacuum pump and 1 atm of D_2 was added. The D_2 pressure was measured from the regulator on the D_2 tank. The valve on the cylinder was closed and the D_2 gas remaining in the system was evacuated. The system was again isolated from the vacuum and over 1 atm of H_2 was added to the system (again the pressure was measured with the regulator). The valve to the cylinder was opened so that H_2 could enter. The overpressure of H_2 ensured that when the valve to the cylinder was opened, H_2 flowed in and D_2 was prevented from leaving. The total pressure on the system was raised to 2 atm by

adjusting the regulator on the H_2 supply tank. The valve on the mixture cylinder was closed (it now contained 1 atm of H_2 and 1 atm of D_2) and the system was evacuated. The cylinder was removed from the vacuum system and put into our setup according to Fig. 3.1.

3.4 Breakthrough Experiment Procedure

The aim of this project was to learn about breakthrough experiments and build a system for conducting them with MOF samples at various temperatures. Many experiments were conducted as the system was built to test the behavior of its components and gain an understanding of the behavior of our MOFs under flow-through conditions. The flow meter was the most recent addition to the system. Before adding it, we conducted pseudo breakthrough experiments, at constant pressure instead of constant flow. These experiments were useful for qualitative analysis of the MOFs but could not be used for any quantitative measurements, as the input quantity of gas was unknown.

Fig. 3.4 shows the steps of our current procedure for a 2-component breakthrough experiment along with the typical mass spectrometer data from each step. Initially, the system is completely evacuated, the 3-way valve is set to direct the flow through the sample, valve 1 is closed, and both the mass spectrometer and vacuum are running. The mass spectrometer software is recording the flow rate upstream and pressure downstream from the sample. The base H_2 signal (the background) is measured, an indication how much of the H_2 signal throughout the experiment is due to water in the system instead of the H_2 in the feed. A flow of the 1:1 H_2/D_2 mixture is established (Fig. 3.4a.), valve 1 is opened and the sample is exposed to the feed (Fig. 3.4b.). Eventually, breakthrough occurs and the effluent flow leaves the system through the mass spectrometer and the vacuum (Fig. 3.4c.). The raw mass spec data

corresponding with each step is shown in Fig. 3.4d. This procedure will be adjusted in the future when we replace the flow meter with a flow controller. Suggestions for future work are further outlined in Ch. 5.

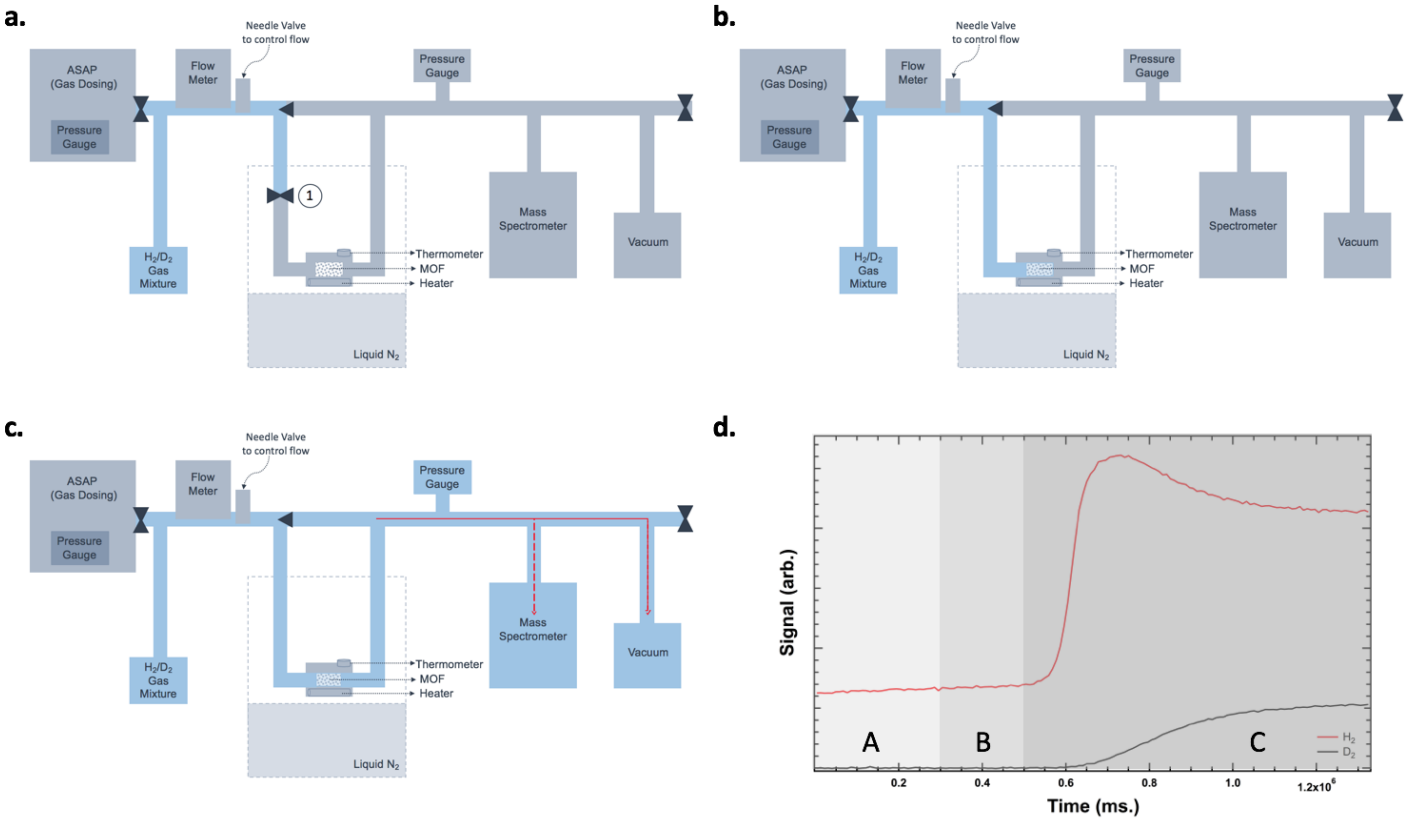

Figure 3.4: **a**. Feed flow is established and H_2 background is measured. **b**. Valve 1 is opened, feed is adsorbed by MOF column. **c**. Breakthrough occurs and the effluent flow is sampled by the mass spectrometer or evacuated. **d**. Raw mass spectrometer data from a typical breakthrough experiment (H_2 signal is red, D_2 is black). Region **A** corresponds to data taken during Step **a**., etc.

3.5 Data Acquisition and Treatment

All data were acquired with a Hiden HPR-20 Quadrupole Mass Spectrometer and corresponding MASoft 7 Professional software. Fig. 3.5 shows raw breakthrough experiment data produced by this mass spectrometer. The following subsections

outline the typical treatment of these data with the analysis software Igor Pro 6.37. Unless otherwise noted, all data in this thesis was treated as follows.

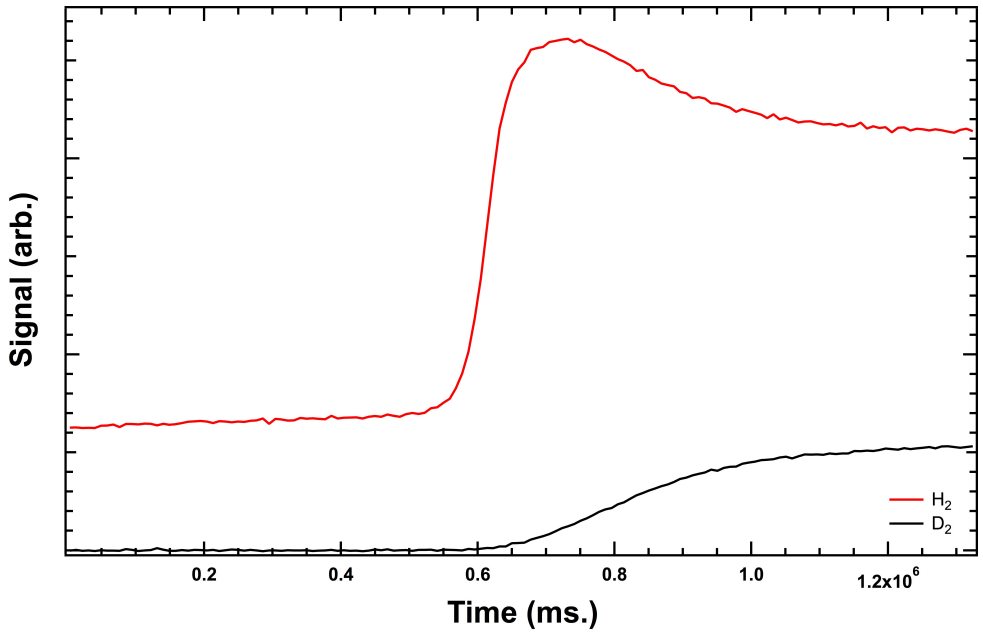

Figure 3.5: Raw data acquired with a mass spectrometer during a breakthrough experiment.

3.5.1 Time Offset

Data is collected with the mass spectrometer before the actual breakthrough experiment begins to determine a baseline for the H_2 signal. t=0 is subsequently defined as the time corresponding to the point at which the column of MOF is first exposed to the gas mixture (when valve 1 in Fig. 3.4a. is opened). Fig. 3.6 shows the data on the adjusted time scale.

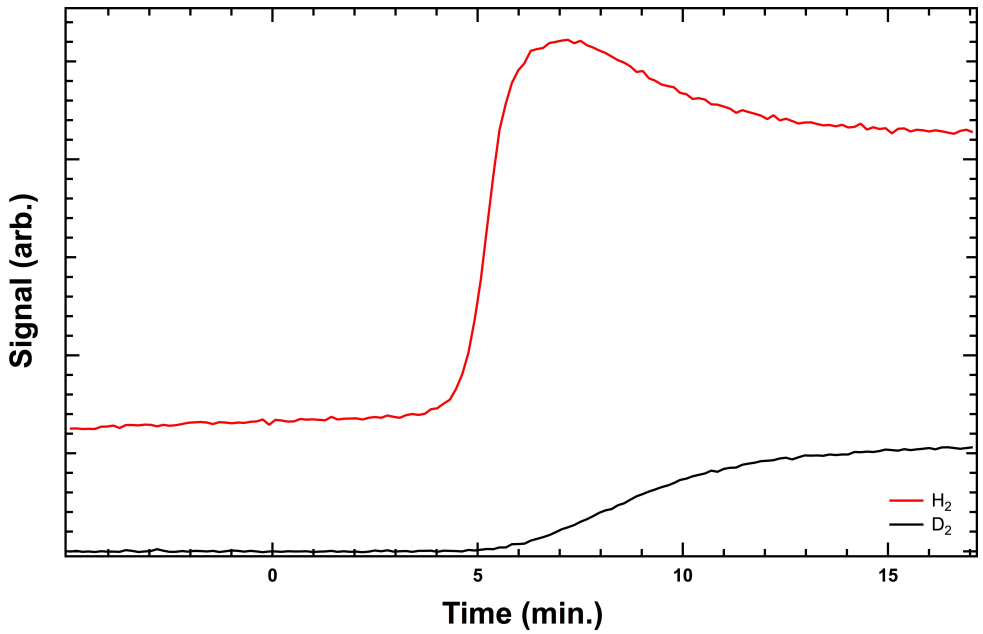

Figure 3.6: Breakthrough data with time adjustment.

3.5.2 H_2 Background

There is a significant hydrogen background in our data attributed to water in our system that is ionized in the mass spectrometer, producing H_2^+ ions that contribute to the signal of the H_2 gas[47]. The background fluctuates daily depending on factors like the humidity of the lab and how extensively the system has been evacuated before an experiment. At the beginning of each experiment, the current hydrogen background is measured. Fig. 3.7a shows a linear fit to the hydrogen background. The background is measured in the few minutes preceding the beginning of the breakthrough experiment, when the signal has stabilized. The fit line is subtracted from the raw data to remove the H_2 background (Fig. 3.7b).

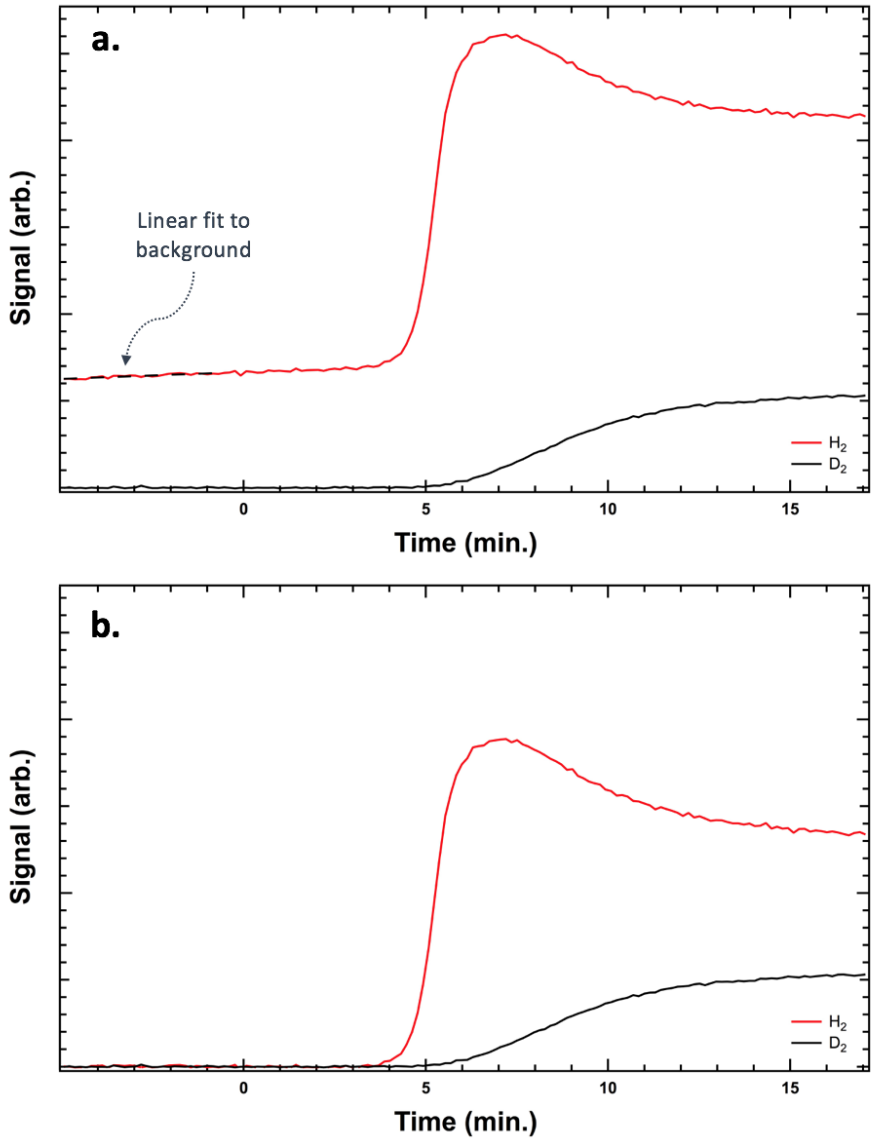

Figure 3.7: **a**. Linear fit to H_2 background. **b**. Fit line is subtracted from raw data to eliminate the H_2 background.

3.5.3 D_2 Scaling

Our mass spectrometer has a higher sensitivity to H_2 than D_2, which leads to a difference in the signal intensity of these two isotopes that is not due to a difference in their concentration. Fig. 3.8 displays this effect for a 1:1 H_2/D_2 mixture at various low pressures that are comparable to the pressure of the effluent flow during our

breakthrough experiments. The H_2 background has been removed from these data. For our mass spectrometer, under 100mbar, the relative sensitivity of H_2 to D_2 is between 2 and 3 (Fig. 3.8 Inset). One factor that may account for the difference in sensitivity is that heavier masses have lower transmission rates[48]. Therefore, fewer D_2^+ than H_2^+ ions make it through the mass filter to the detector. It is near impossible to predict relative sensitivity factors for a mass spectrometer because each instrument is unique[48]. Determining the relative sensitivity from data is more reliable.

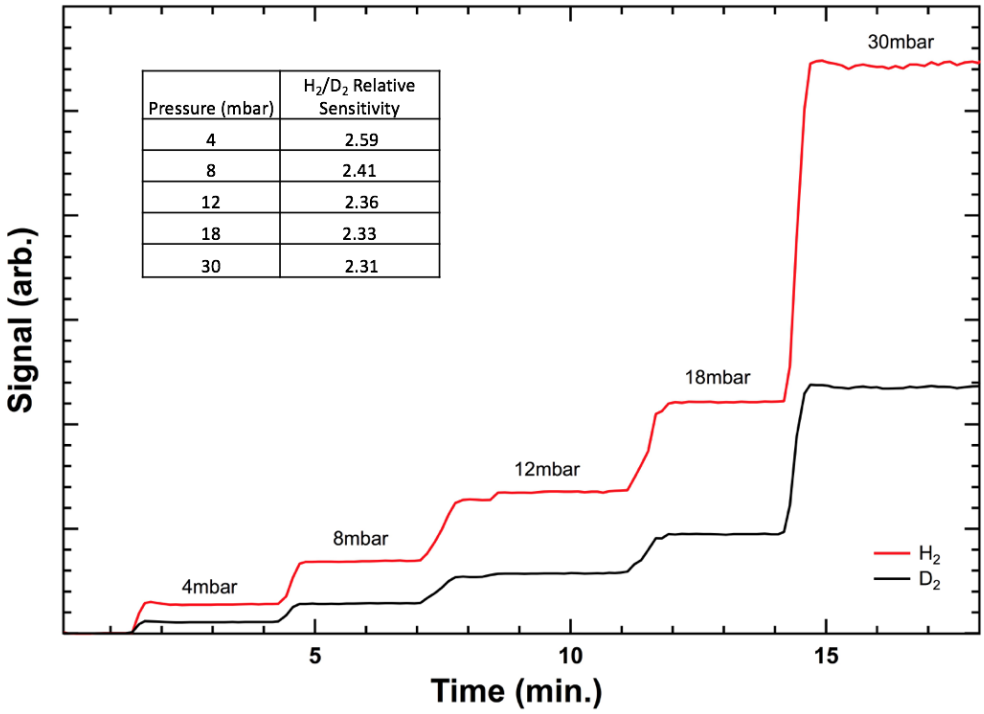

Figure 3.8: Mass spectrometer signal (after subtracting the H_2 background) for 1:1 H_2/D_2 mixture at multiple pressures comparable to those of the effluent flow during our breakthrough experiments. Inset table: Calculation of H_2 (red) to D_2 (black) relative sensitivity; relative sensitivity decreases as pressure increases.

In this work, a 1:1 H_2/D_2 mixture is always used as the feed and data are taken until equilibrium is reached in each breakthrough experiment. The H_2 and D_2 signals at equilibrium should presumably be the same and can be used as a measure of the relative sensitivity of H_2/D_2.

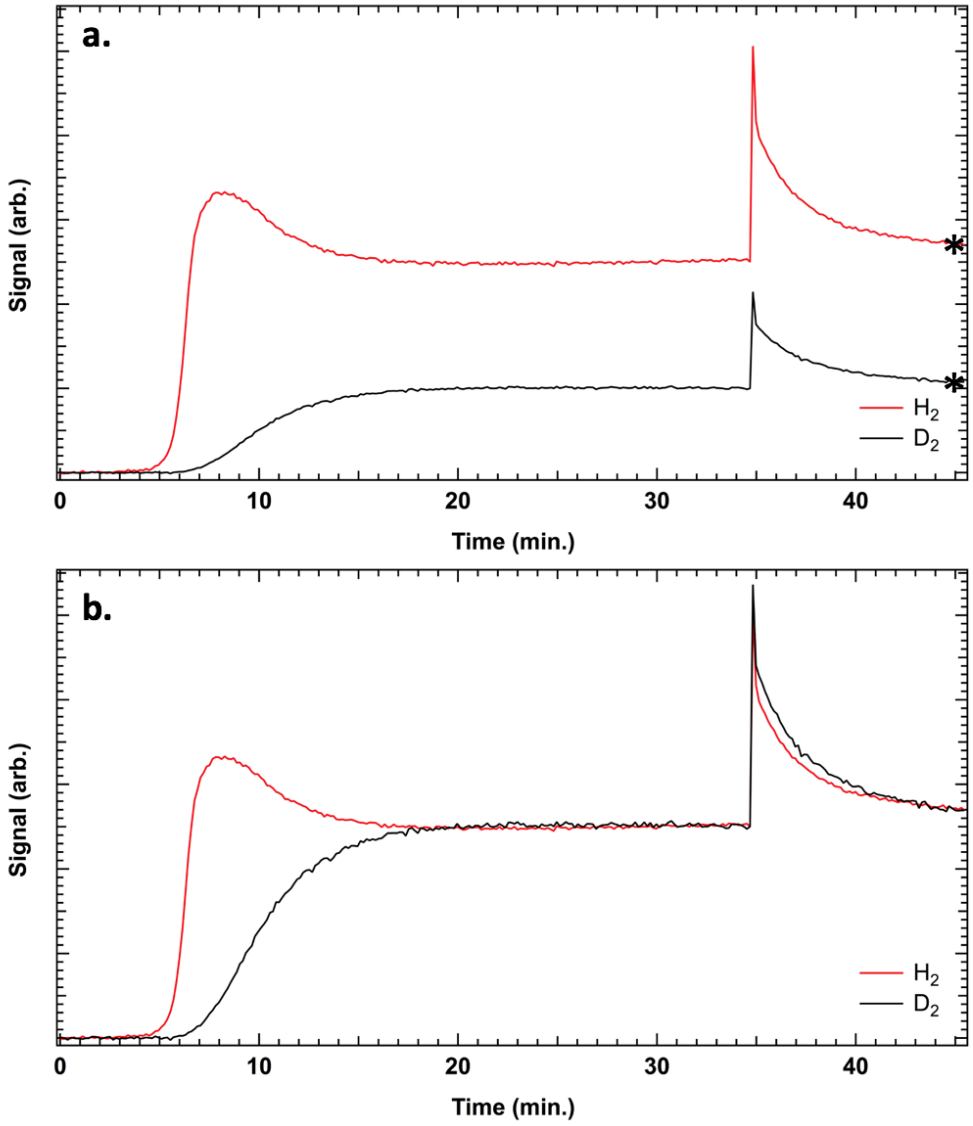

Figure 3.9: **a**. Data from a breakthrough experiment that reached equilibrium. At 35 mins, the H_2 and D_2 signals from the input feed were measured. The relative sensitivity of H_2 to D_2 was calculated using the data at *. **b**. The data were scaled by this value. It is evident that the relative sensitivity of H_2 to D_2 at equilibrium is the same as the relative sensitivity in the input feed.

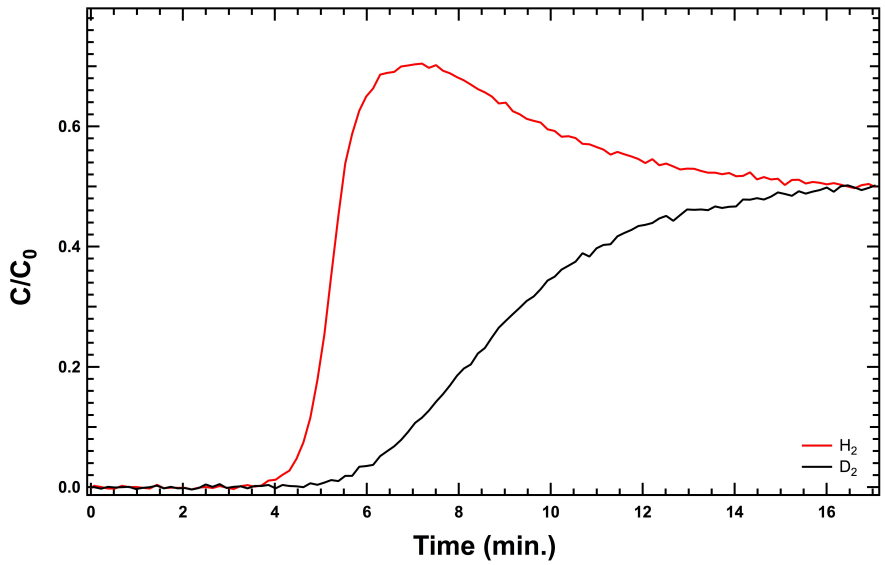

Figure 3.10: D_2 signal was multiplied by 2.53 so that at equilibrium the D_2 signal is equal to the H_2 signal. This relative sensitivity is approximately consistent with Fig. 3.8. Additionally, MS Signal was converted to C/C_0 ratio.

Fig. 3.9a. shows the data from a breakthrough experiment that reached equilibrium around 20 minutes. At 35 minutes, the sample was bypassed by adjusting the 3-way valve (Fig. 3.1), and the input feed (the 1:1 H_2/D_2 mixture) was directed straight into the mass spectrometer. The relative sensitivity of the H_2 to D_2 signal was calculated from the two marked data points (*). When the D_2 data were scaled by this ratio (Fig. 3.9b.), the H_2 and D_2 signals at equilibrium were also equal, indicating that the relative intensity of H_2 to D_2 can be calculated from the mass spectrometer signals at equilibrium. The D_2 data in Fig. 3.10 and Ch. 4 were scaled according to the H_2/D_2 relative sensitivity at equilibrium.

Additionally, all the data were converted from arbitrary mass spectrometer units to C/C_0 by dividing each individual scaled mass spectrometer signal by the combined scaled mass spectrometer signal at equilibrium. C and C_0 are the time-dependent concentrations of the individual component and the total input concentration, re-

spectively. With our 1:1 mixture, both components should come to 0.5 C/C_0 at equilibrium.

Chapter 4

Results

4.1 Breakthrough Analysis of Co-MOF-74

The following data were obtained with a 71 mg sample of Co-MOF-74 in the sample cell pictured in Fig. 3.2a. The sample length was estimated to be around 0.75 cm long, assuming the density of the column was close to Co-MOF-74 crystalline density ($1.14 g/cm^3$) and the width of the column was the same as the inner diameter of the cell (0.33cm). Breakthrough experiments were conducted at room temperature (Fig. 4.1a.) and 77K (4.1b.). At room temperature, the breakthrough time for both isotopes was immediate and there was no observable difference in their behavior. This is expected, as Co-MOF-74 does not significantly adsorb hydrogen and thus does not display the CAQS effect at room temperature. Comparatively, there is observable separation between the isotopes when a breakthrough experiment is conducted with the sample cell submerged in liquid nitrogen. The breakthrough times in Fig. 4.1b. are not immediate, indicating that adsorption of both isotopes occurs at 77K. The difference in H_2 and D_2 breakthrough time and the presence of the H_2 overshoot indicate that Co-MOF-74 preferentially adsorbs D_2 over H_2. These data confirmed

our expectations that separation in Co-MOF-74 is temperature dependent and that D_2 is preferentially adsorbed over H_2.

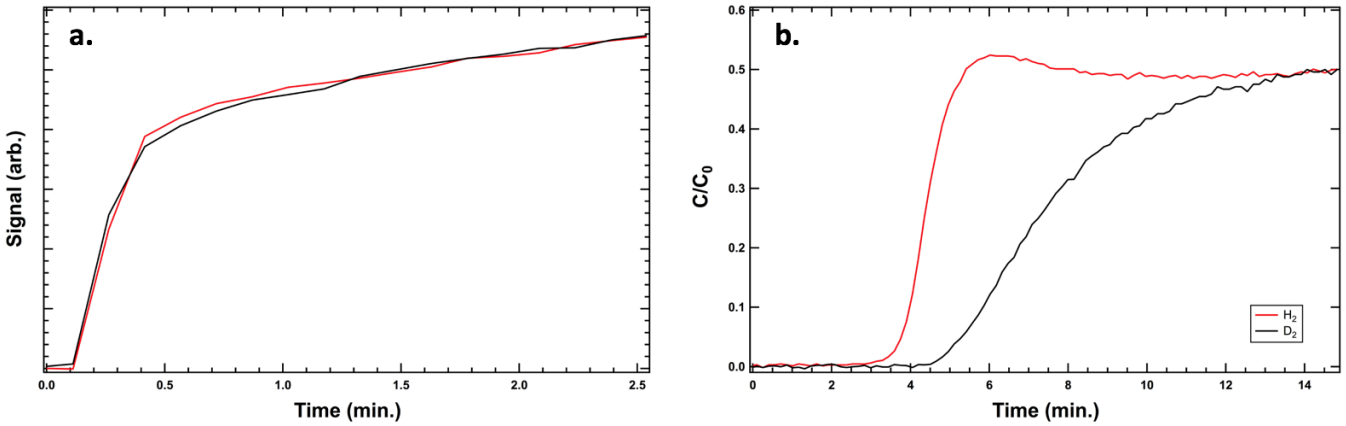

Figure 4.1: Co-MOF-74 Breakthrough Experiment with a 1:1 H_2/D_2 mixture at **a**. room temperature, 0.28 sccm, 3 mbar output pressure (03/29/19) and **b**. 77K, 0.22 sccm, 4 mbar output pressure (03/30/19).

Another interesting, though expected, effect was observed after degassing the Co-MOF-74 sample. Over time, the MOF open-metal adsorption sites can be blocked by water adsorption. Fewer sites are then available for hydrogen adsorption and adsorption separation effects diminish. Co-MOF-74 can be regenerated by heating the sample to 200°C and flowing nitrogen gas through it overnight[22]. Fig. 4.2 shows data from experiments done before and after degassing our sample.

The longer H_2 and D_2 breakthrough times as well as the enlargement of the overshoot region are evidence of an increase in the number of available adsorption sites, primarily the highly-selective open-metal sites. We see additional evidence of an increase in the number of highly-selective adsorption sites when calculating the selectivity. The selectivity, calculated with Eq. 2.8, increased from 1.8 to 2.3 after degassing the sample.

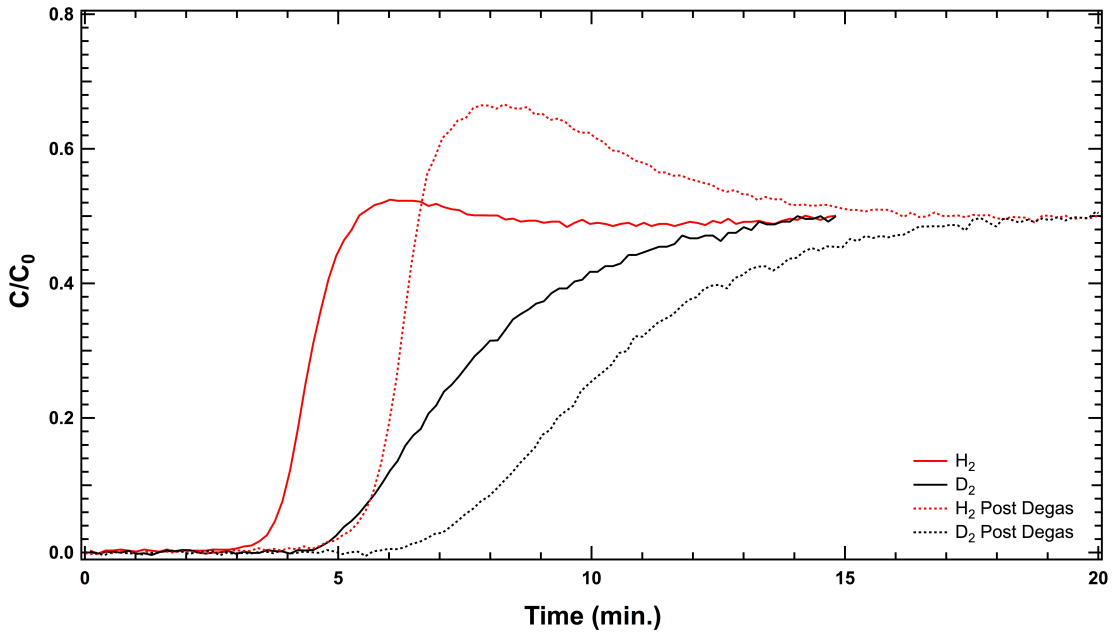

Figure 4.2: Co-MOF-74 breakthrough experiment at 77K before and after degas (03/30/19, 0.22 sccm, 4 mbar output pressure and 04/01/19, 0.22 sccm, 4 mbar output pressure).

In order to evaluate the reproducibility uncertainty in the selectivity measurements, a second breakthrough experiment was conducted with the regenerated MOF at 77K (Fig. 4.3). The two data sets were taken successively without altering the setup. The breakthrough time for H_2 was around 4 minutes and the difference in breakthrough time between H_2 and D_2 was around 2 minutes for both experiments. The shape of the data differ slightly as time progressed, possibly due to a small difference in flow rates. The needle valve controlling the flow was not changed between experiments. However, the flow meter measured a flow rate of 0.26 sccm (standard cubic centimeters per minute) during the initial experiment and 0.22 sccm during the repeat experiment. The calculated selectivity was 2.3 in the first run and 2.5 in the second. This difference implies that the reproducibility uncertainty in our selectivity measurements is around 10%.

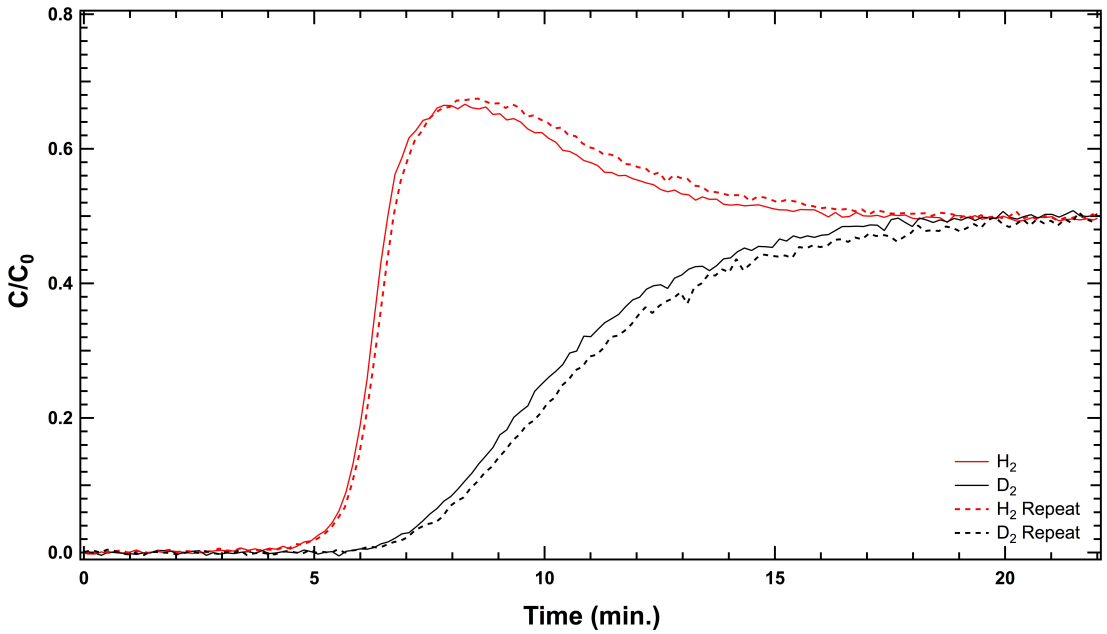

Figure 4.3: Co-MOF-74 breakthrough experiment at 77K (04/01/19, 0.26 sccm, 4 mbar output pressure). Experiment was repeated to evaluate reproducibility ((04/01/19, 0.22 sccm, 4 mbar output pressure).

The selectivity of Co-MOF-74 at 77K has been measured directly [14] and with IAST analysis of single component isotherms[17]. In both cases it was found to be 3.3. Two factors that may contribute to our selectivity being lower than 3.3 are channeling and sample temperature change due to the heat of adsorption. Channeling would reduce selectivity because gas would pass through the sample without being adsorbed (a process that has a selectivity of 1). Additionally, if the heat released upon adsorption is enough to heat the MOF significantly, measured selectivity may decrease because selectivity decreases as temperature increases with our adsorption separation mechanism. In the future, we would like to directly measure the temperature of our MOF column to see if we observe any change due to the heat of adsorption.

4.2 Breakthrough Analysis of Cu(I)-MFU-4*l*

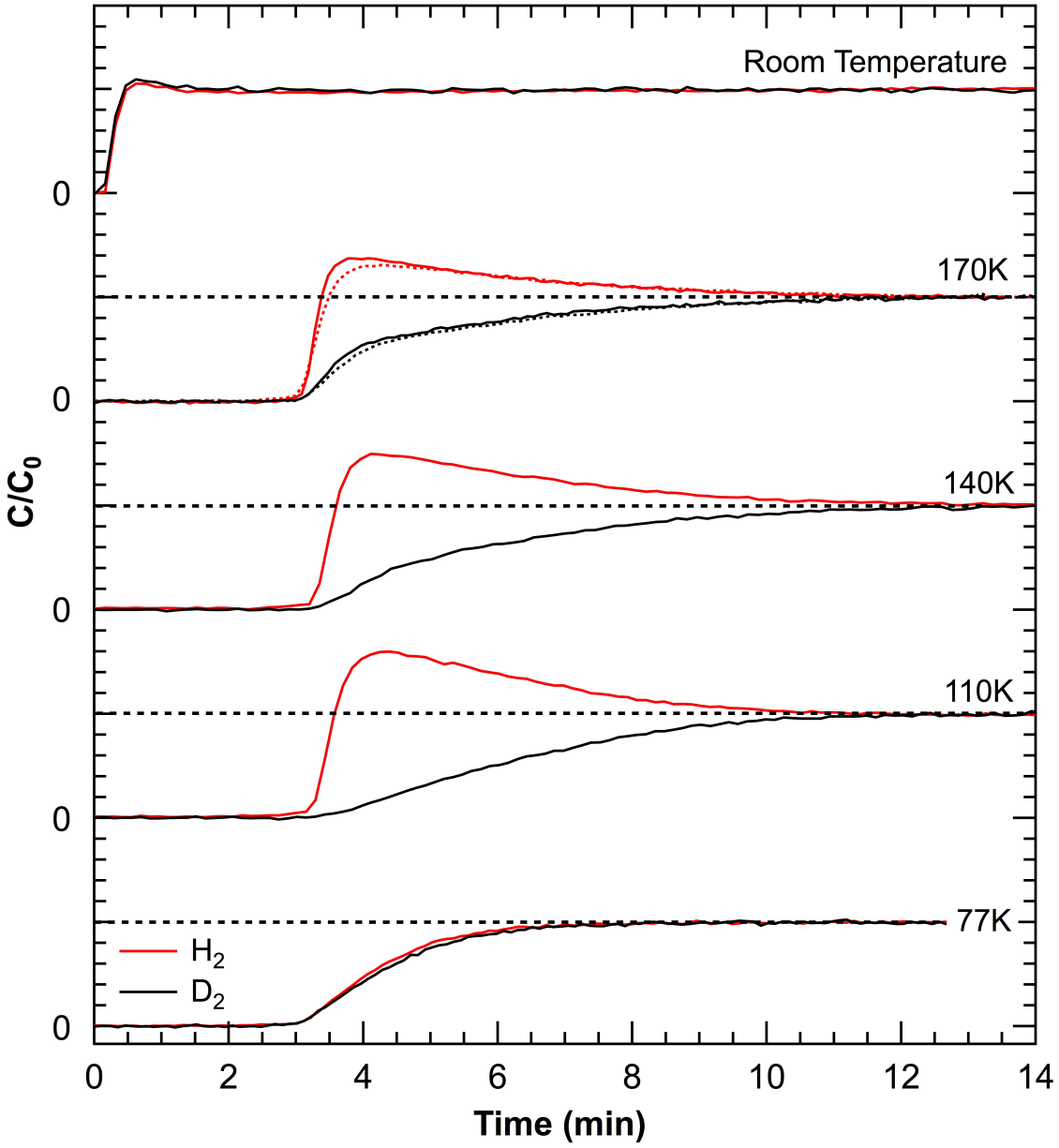

Figure 4.4: Cu(I)-MFU-4*l* breakthrough experiments at 77K, 110K, 140K, 170K and room temperature (04/02/19). The dotted lines mark 0.5 C/C_0 for each data set.

All data in this section were obtained with a 21.8 mg sample of Cu-MFU-4*l* in the temperature controlled cell pictured in Fig. 3.2b. The length of the column was approximately 0.5 cm (calculated from the crystalline density of MFU-4*l*, 0.56 g/cm^3[23],

and the diameter of the sample cell, 0.33 cm). Fig. 4.4 shows data from breakthrough experiments conducted at five different temperatures: 77K, 110K, 140K, 170K and room temperature. The flow rate was not the same across these experiments so the data were time-scaled to the same H_2 breakthrough time for comparison. At room temperature, breakthrough was immediate and the isotopes behaved identically as expected. At 170K, the classic breakthrough shape was observed. The area between the H_2 and D_2 curves increased at 140K and 110K, a result of an increase in selectivity at low temperature. However, at 77K adsorption occurred but there was no preferential adsorption of D_2 (indicated by the identical behavior between H_2 and D_2). This behavior has been observed in our previously conducted adsorption experiments (that have not been published) and indicates that there may be some structural change in Cu(I)-MFU-4*l* below 110K that prevents preferential adsorption of D_2. We are interested in investigating this behavior in future work.

Table 4.1 shows the calculated selectivity at each temperature. An evaluation of reproducibility was done at 170K; the reproducibility uncertainty in the selectivity was 1%. Ref. [3] predicted a selectivity of Cu(I)-MFU-4*l* of 3.6 at 160K and 5.0 at 140 K. Comparatively, our calculated selectivities are low for their temperatures. Channeling and isosteric heat of adsorption may play a role in reducing our measured selectivity for these data, as with the data for Co-MOF-74. We hope to develop experiments in the future to investigate these phenomena in our system.

Temperature	Selectivity
170 K	2.4
140 K	3.6
110 K	4.1
77 K	1.0

Table 4.1: Cu(I)-MFU-4*l* selectivity measurements at 77K, 110K, 140K, and 170K.

Cu(I)-MFU-4l at 170K had a similar selectivity to Co-MOF-74 at 77K (2.6 compared to 2.3/2.5), and a higher selectivity below 170K. This indicates that separation with Cu(I)-MFU-4l may be comparatively more energy efficient since selectivities higher than 2.4 can be achieved at temperatures warmer than 77K.

Chapter 5

Conclusion

The intent of this work was to design, build, and test a flow-through system to study adsorption separation of hydrogen isotopes in metal-organic frameworks. Breakthrough experiments were conducted to investigate a zero-point energy-based separation mechanism in two MOFs: Co-MOF-74 and Cu(I)-MFU-4*l*. We saw preferential adsorption of D_2 over H_2 in Co-MOF-74 at 77K and Cu(I)-MFU-4*l* at 170K, 140K, and 110K. This behavior was absent in Cu(I)-MFU-4*l* at 77K. Minimal adsorption occurred in both MOFs at room temperature. A selectivity around 2.4 was measured in Co-MOF-74 at 77K (reproducible to 10%). Selectivities of 2.4 (170K), 3.6 (140K, reproducible to 1%) and 4.1 (110K) were measured in Cu(I)-MFU-4*l*. All measured selectivities were lower than comparable literature values. We hope to make improvements to our system and methods to more accurately measure the selectivity. Notably, all measured selectivities were higher than the selectivity of the Girdler Sulfide method (1.3) and cryogenic distillation (1.5), the two industrial hydrogen isotope separation processes we are trying to improve on.

This new system gives us the capability to study adsorption and kinetic separation of hydrogen isotopes in metal-organic frameworks going forward. We hope that our

work will inform the development of efficient, environmentally sustainable separation processes.

5.1 Future Work

Equipment upgrades to our system are already under way. The flow meter will be replaced with a flow controller so that consistent flow rates can be maintained across breakthrough experiments. A flow meter may be added after the sample so that the amount of gas adsorbed in the MOF (the difference in flow rates) can be measured. This would also allow us to evaluate the flow adsorption capacity of our MOF samples. Currently, the system is under vacuum before each breakthrough experiment, which leads to a large pressure drop across the MOF column when the experiment is started and the feed gas enters the column. To reduce this pressure drop, we would like to run a helium flow through the sample and then flip to the adsorbate feed to start a breakthrough experiment. As mentioned in Ch. 4, we are concerned that the MOF column may be heating up as gas adsorbs. A temperature probe should be added to the inside of our MOF column so that this effect can be studied. We are also concerned that the adsorbate feed may be heating the MOF since it is at room temperature in our current system. Developing a method to cool the feed before it enters the MOF column is an important future improvement.

We would also like to improve our MOF column synthesis, which could reduce channeling during our experiments and improve selectivity measurements. Appendix A outlines suggestions, from private communications with Orhan Talu at Cleveland State University and Rebecca Siegelman at University of California-Berkeley, for making the column composition more uniform and better suited for breakthrough experiments.

We hope that upgrading our system and methods will enable us to more accurately measure selectivity and determine the uncertainty in this measurement. We would like to do more rigorous data analysis, including evaluating fits to our data with the kinetic breakthrough models suggested in Ch. 2. A final consideration for future work is that we are primarily interested in recovering D_2, the more preferentially adsorbed species, which requires additional steps beyond a simple flow-through process. Pressure and temperature swing adsorption could be investigated as methods of isolating D_2.

Appendix A

MOF Column Synthesis Notes

In the future, our MOF columns should be made according to more specific parameters than those used in this work. Orhan Talu, at Cleveland State University, provided some guidance in creating the optimal MOF column for a breakthrough experiment during our lab visit with him and via email. The length of the pellet should be between 6 and 10 times its diameter (the diameter was 0.33 cm in this work). A ratio beyond 10 leads to a significant pressure drop across the sample, which is undesirable. A ratio below 6 results in a short mass transfer region which can cause channeling (when the flow bypasses the majority of MOF particles). The length/diameter ratio of the MOF columns used in this work was around 3.

Another important ratio is that of the cell diameter to the MOF particle diameter. Talu suggests that this ratio be over 10 and in general, the larger the better. During my visit to her lab, Rebecca Siegelman, a PhD candidate in Jeff Long's lab at the University of California-Berkeley, outlined a method for "pelletizing" MOF samples so that the particles are 10% of the diameter of the column (Fig. A.1). The MOF powder is pressed into a disk (A.1a.) and then filtered through two copper sieves with different sized gratings so that the particles caught in the middle are around 10% of the column diameter (A.1b.). These particles are the ones used to create the column.

Both Talu and Siegelman emphasized that the MOF sample should only be pressed gently, so as not to damage its crystal structure. Ideally, the kinetic and adsorptive behavior of the sample should be evaluated before and after "pelletization" to ensure that the properties of the sample have not changed.

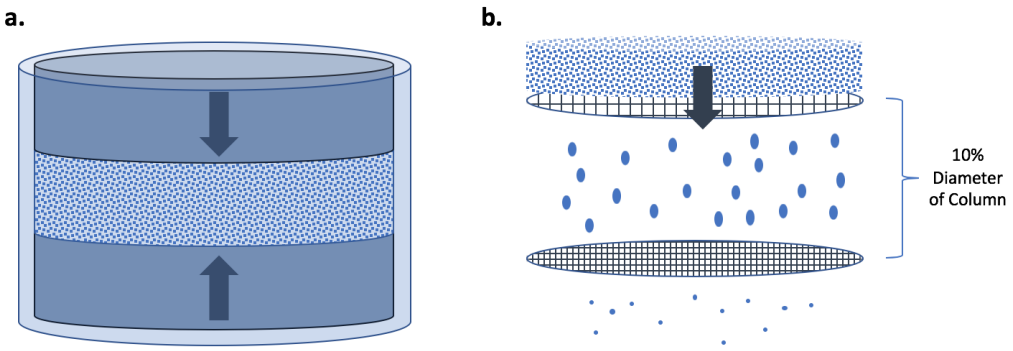

Figure A.1: Method of creating MOF particles that are 10% of the column diameter. **a**. Press MOF powder into disk. **b**. Filter disk through two sieves of different sizes so that the particles caught in the middle are approximately 10% of the column diameter.

Bibliography

[1] U.S. Energy Information Administration. February 2019 Monthly Energy Review. eia.gov, February 2019.

[2] D.S. Sholl and R.P. Lively. Seven chemical separations to change the world. *Nature*, 532:435–437, April 2016.

[3] I. Weinrauch, I. Savchenko, D. Denysenko, S. M. Souliou, H-H Kim, M. Le Tacon, L. L. Daemen, Y. Cheng, A. Mavrandonakis, A. J. Ramirez-Cuesta, D. Volkmer, G. Schtz, M. Hirscher, and T. Heine. Capture of heavy hydrogen isotopes in a metal–organic framework with active Cu(I) sites. *Nature Communications*, 8:14496, March 2017.

[4] I. Friedman. Deuterium content of natural waters and other substances. *Geochimica et Cosmochimica Acta*, 532(1–2):89–103, August 1953.

[5] S. Kaufman and W.F. Libby. The Natural Distribution of Tritium. *Physical Review*, 93(6):1337–1344, March 1954.

[6] H.K. Rae. Separation of Hydrogen Isotopes. *American Chemical Society*, 68:1–26, 1978.

[7] M. Omidvar, H. Nguyen, J. Liu, and H. Lin. Sorption–enhanced membrane materials for gas separation: a road less traveled. *Current Opinion in Chemical Engineering*, 20:50–59, June 2018.

[8] P. Bernardo, E. Drioli, and G. Golemme. Membrane Gas Separation: A Review/State of the Art. *Ind. Eng. Chem. Res.*, 48(10):4638–4663, April 2009.

[9] H. Li, K. Wang, Y. Sun, C. T. Lollar, J. Li, and H.C. Zhou. Recent advances in gas storage and separation using metalorganic frameworks. *Materials Today*, 21(2):108–121, March 2018.

[10] G. Han, Y. Gong, H. Huang, D. Cao, X. Chen, D. Liu, and C. Zhong. Screening of Metal–Organic Frameworks for Highly Effective Hydrogen Isotope Separation by Quantum Sieving. *ACS Applied Materials & Interfaces*, 10(38):32128–32132, September 2018.

[11] J.Y. Kim, H. Oh, and H.R. Moon. Hydrogen Isotope Separation in Confined Nanospaces: Carbons, Zeolites, Metal–Organic Frameworks, and Covalent Organic Frameworks. *Adv. Mater.*, page 1805293, December 2018.

[12] H. Oh and M. Hirscher. Quantum Sieving for Separation of Hydrogen Isotopes Using MOFs. *Eur. J. Inorg. Chem.*, 2016(27):89–103, June 2016.

[13] M.P. Suh, H.J. Park, T.K. Prasad, and D.W. Lim. Hydrogen Storage in Metal–Organic Frameworks. *Chemical Reviews*, 112(2):782–835, December 2012.

[14] N. Zhang. Hydrogen Isotope Separation in Metal–Organic Frameworks. Bachelor's thesis, Oberlin College, March 2018.

[15] S.A. FitzGerald, K. Shinbrough, K.H. Rigdon, J.L.C. Rowsell, M.T. Kapelewski, S.H. Pang, K.V. Lawler, and P.M Forster. Temperature–Programmed Desorption for Isotope Separation in Nanoporous Materials. *J. Phys. Chem. C*, 122(4):1994–2001, January 2014.

[16] K. Shinbrough. Infrared and Thermal–Desorption Spectroscopy of H_2 and D_2 in Metal Organic Frameworks. Bachelor's thesis, Oberlin College, March 2017.

[17] S.A. FitzGerald, C.J. Pierce, J.L.C. Rowsell, E.D. Bloch, and J.A. Mason. Highly Selective Quantum Sieving of D2 from H2 by a Metal–Organic Framework As Determined by Gas Manometry and Infrared Spectroscopy. *J. Am. Chem. Soc.*, 135(25):9458–9464, May 2013.

[18] N.L. Rosi, J. Kim, M. Eddaoudi, B. Chen, M. O'Keeffe, and O.M. Yaghi. Rod Packings and Metal–Organic Frameworks Constructed from Rod-Shaped Secondary Building Units. *Journal of the American Chemical Society*, 127(5):1504–1518, January 2005.

[19] D. Denysenko, M. Grzywa, J. Jelic, K. Reuter, and D. Volkmer. Scorpionate–Type Coordination in MFU–4l Metal–Organic Frameworks: Small–Molecule Binding and Activation upon the Thermally Activated Formation of Open Metal Sites. *Angew. Chem. Int. Ed*, 53(23):5832–583, May 2014.

[20] M.T. Kapelewski, S.J. Geier, M.R. Hudson, D. Stck, J.A. Mason, J.N. Nelson, D.J. Xiao, Z. Hulvey, E. Gilmour, S.A. FitzGerald, M. Head-Gordon, C.M. Brown, and J.R. Long. M2(m-dobdc) (M = Mg, Mn, Fe, Co, Ni) Metal–Organic Frameworks Exhibiting Increased Charge Density and Enhanced H2 Binding at the Open Metal Sites. *Langmuir*, 24(9):4772–4777, March 2008.

[21] J.A. Villajos, G. Orcajo, C. Martos, J. Á. Botas, J. Villacaas, and G. Calleja. Co/Ni mixed-metal sited MOF–74 material as hydrogen adsorbent. *International Journal of Hydrogen Energy*, 40(15):5346–5352, 2015.

[22] S. A. FitzGerald, B. Burkholder, M. Friedman, J.B. Hopkins, C.J. Pierce, J.M. Schloss, B. Thompson, and J.L.C. Rowsell. Metal–Specific Interactions of H_2

Adsorbed within Isostructural Metal–Organic Frameworks. *J. Am. Chem. Soc.*, 133(50):20310–20318, November 2011.

[23] D. Denysenko, M. Grzywa, M. Tonigold, B. Streppel, I. Krkljus, M. Hirscher, E. Mugnaioli, U. Kolb, J. Hanss, and D. Volkmer. Elucidating Gating Effects for Hydrogen Sorption in MFU–4–Type Triazolate–Based Metal–Organic Frameworks Featuring Different Pore Sizes. *Chemistry – A European Journal*, 17(6):1837–1848, 2011.

[24] B. Barnett. Formation of Three-Coordinate Cu(I) Centers in MFU-4*l*. Private Communications.

[25] Y. Wang and D. Zhao. Beyond Equilibrium: Metal–Organic Frameworks for Molecular Sieving and Kinetic Gas Separation. *Cryst. Growth Des.*, 2017(17):2291–2308, April 2017.

[26] J.J.M. Beenakker, V.D. Borman, and S.Yu. Krylov. Molecular transport in subnanometer pores: zero-point energy, reduced dimensionality and quantum sieving. *Chemical Physics Letters*, 232(4):379–382, 1995.

[27] H. Oh, K.S. Park, S.B. Kalidindi, R.A. Fischer, and M. Hirscher. Quantum cryo–sieving for hydrogen isotope separation in microporous frameworks: an experimental study on the correlation between effective quantum sieving and pore size. *J. Mater. Chem. A*, 1(10):3244–3248, 2013.

[28] B. Chen, X. Zhao, A. Putkham, K. Hong, E.B. Lobkovsky, E.J. Hurtado, A.J. Fletcher, and K.M. Thomas. Surface Interactions and Quantum Kinetic Molecular Sieving for H2 and D2 Adsorption on a Mixed Metal–Organic Framework Material. *Journal of the American Chemical Society*, 130(20):6411–6423, 2008.

[29] J. Teufel, H. Oh, M. Hirscher, M. Wahiduzzaman, L. Zhechkov, A. Kuc, T. Heine, D. Denysenko, and D. Volkmer. Mfu–4 – a metal-organic framework for highly effective h(2)/d(2) separation. *Advanced Materials*, 25(4):635–639, January 2013.

[30] J. Liu, W. Xia, W. Mu, P. Li, Y. Zhao, and R. Zou. New challenge of metal–organic frameworks for high–efficient separation of hydrogen chloride toward clean hydrogen energy. *J. Mater. Chem. A*, 3(10):5275–5279, 2015.

[31] D. Britt, H. Furukawa, B. Wang, T.G. Glover, and O.M. Yaghi. Highly efficient separation of carbon dioxide by a metal–organic framework replete with open metal sites. *Proceedings of the National Academy of Sciences*, 106(49):20637–20640, 2009.

[32] R. Krishna and J.R. Long. Screening metal–organic frameworks by analysis of transient breakthrough of gas mixtures in a fixed bed adsorber. *The Journal of Physical Chemistry C*, 115(26):12941–12950, 2011.

[33] A.J.W. Physick, D.J. Wales, S.H.R. Owens, J. Shang, P.A. Webley, T.J. Mays, and V.P. Ting. Novel low energy hydrogen-deuterium isotope breakthrough separation using a trapdoor zeolite. *Chemical Engineering Journal*, 288:161–168, 3 2016.

[34] M. S. P. Silva, M. A. Moreira, A. F. P. Ferreira, J. C. Santos, V. M. T. M. Silva, P. S Gomes, M. Minceva, J. P. B. Mota, and A. E. Rodrigues. Adsorbent evaluation based on experimental breakthrough curves: Separation of *p*-xylene from c_8 isomers. *Chemical Engineering & Technology*, 35(10):1777–1785, 2012.

[35] H.C. Thomas. Heterogeneous ion exchange in a flowing system. *Journal of the American Chemical Society*, 66(10):1664–1666, 1944.

[36] Y.H. Yoon and J.H. Nelson. A theoretical model for respirator cartridge service life. *Am. Ind. Hyg. Assoc. J.*, 66(8):509–516, 1984.

[37] G. S. Bohart and E. Q. Adams. Some aspects of the behavior of charcoal with respect to chlorine. *Journal of the American Chemical Society*, 42(3):523–544, 1920.

[38] Z. Chowdhury, S. Zain, A. Rashid, R. Rafique, and K. Khalisanni. Breakthrough curve analysis for column dynamics sorption of Mn(II) ions from wastewater by using mangostana garcinia peel–based granular–activated carbon. *E–Journal of Chemistry*, 2013, January 2013.

[39] A. Ghribi and M. Chlendi. Modeling of fixed bed adsorption: Application to the adsorption of an organic dye. *Asian Journal of Textile*, 1(4):161–171, 2011.

[40] C. Escudero, J. Poch, and I. Villaescusa. Modelling of breakthrough curves of single and binary mixtures of Cu(II), Cd(II), Ni(II) and Pb(II) sorption onto grape stalks waste. *Chemical Engineering Journal*, 217:129–138, 2013.

[41] L. Joss, M. Gazzani, M. Hefti, D. Marx, and M. Mazzotti. Temperature swing adsorption for the recovery of the heavy component: An equilibrium–based shortcut model. *Industrial & Engineering Chemistry Research*, 54(11):3027–3038, 2015.

[42] S. Farooq D.M. Ruthven and K.S. Knaebel. *Pressure Swing Adsorption*. VCH, 1995.

[43] J. Honour. Benchtop mass spectrometry in clinical biochemistry. *Annals of clinical biochemistry*, 40:628–638, December 2003.

[44] LCGC Editors. Quadrupole mass analysers: An introduction. *LCGC Europe*, 25(11):640, November 2012.

[45] I. Tyrer-Tomkinson. Massoft professional version 7 training manual. Hiden Analytical, Issue a: 84.

[46] D. Mukasa. Development of a highly Selective Deuterium-Hydrogen Separation Process. Bachelor's thesis, Oberlin College, April 2019.

[47] R.E. Ellefson, W.E. Moddeman, and H.F. Dylla. Hydrogen isotope analysis by quadrupole mass spectrometry. *Journal of Vacuum Science and Technology*, 18(3):1062–1067, March 1981.

[48] Hiden Analytical. Relative sensitivity: Rs measurements of gases. Technical Report Application Note 282, Warrington, WA5 7UN, England.